Development of an interferometer-based transient two-dimensional infrared Spectrometer

Physics Institute
University of Zürich

Mathias Hausherr
Zürich, June 2011

Master Thesis under guidance of Dr. Jan Helbing in the group of Prof. Dr. Peter Hamm at the Institute of Physical Chemistry.

Contents

Abstract

Transient two-dimensional infrared (T2D IR) spectroscopy extends the advantages of two-dimensional infrared (2D IR) spectroscopy to the investigation of a transient species with picoseconds (ps) time resolution. A T2D IR spectroscopy method based on a 2D Fourier transform (FT) IR spectroscopy method using a collinear pulse-pair pump - probe geometry is introduced. The techniques of 2D and T2D IR spectroscopy are explained before the new setup is described in more detail.
The first measurements using this new T2D IR setup are performed on a well-studied Rhenium complex. Different types of T2D IR pulse sequences are demonstrated and the results are compared with earlier frequency domain experiments. The new T2D and 2D IR spectroscopy setup significantly enhances spectral and temporal resolution without increasing the complexity of the setup and the experimental handling.

1 Introduction

Two-dimensional infrared (2D IR) spectroscopy describes a 3^{rd}-order nonlinear process and was first introduced in 1998 [1] even though its possibility has already been mentioned in 1976. [2] In the last decades several 2D IR spectroscopy setups have been developed. [1,3–8] These setups are usually based on either a frequency domain pump-probe spectroscopy method [1] or a time domain photon-echo spectroscopy method [7]. Fig. 1(a) illustrates a 2D spectrum of a Rhenium complex (Fig. 1(c)) dissolved in dimethylsulfoxide (DMSO) and on top, the linear one-dimensional (1D) Fourier transform infrared (FTIR) spectrum is shown. Linear FTIR spectroscopy measures the absorbance of a sample upon interaction with an electromagnetic radiation. With respect to the 2D IR spectrum, the linear FTIR spectrum describes the diagonal of a 2D IR spectrum. However, in a 2D IR spectrum, peak doublets appear on the diagonal which describe different transitions (not only the absorbance). Furthermore, 2D IR spectra are most known for their off-diagonal peak doublets, the so-called cross-peaks. These cross-peaks are visualized by using two frequency dimensions and illustrate correlations between different vibrational bands which cannot be noticed in a simple 1D FTIR spectrum. $a'(2)$, a'', and $a'(1)$ label the C=O vibrational bands of the Rhenium-complex and the cross-peaks illustrate the correlation between the different C=O bands in Fig. 1(a).

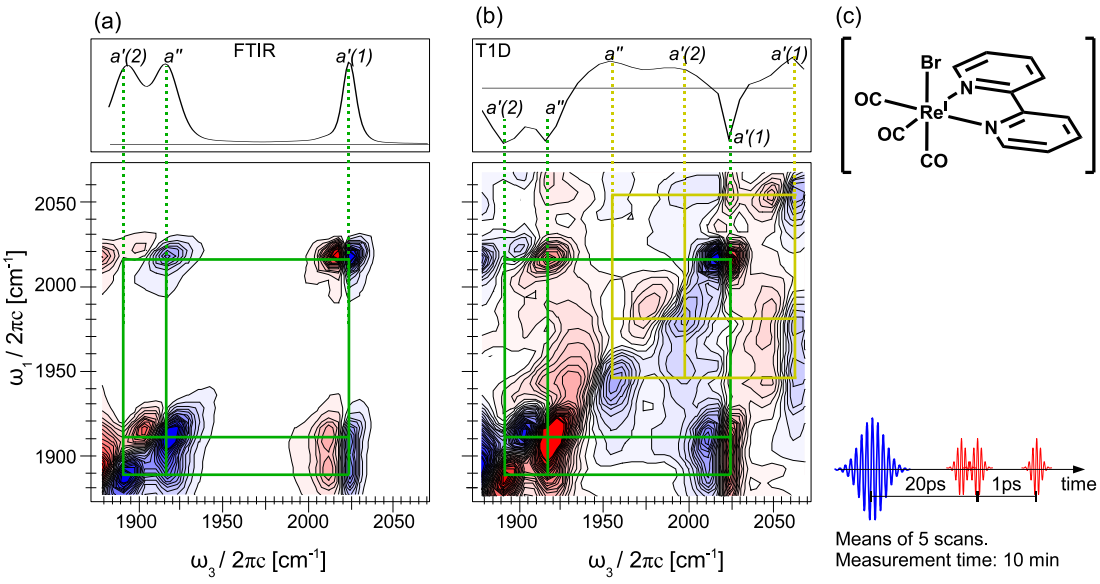

Figure 1: (a) 2D IR spectrum and (b) T2D IR spectrum of a Rhenium-complex (c) dissolved in dimethylsulfoxide.

Besides the coupling between vibrational bands, 2D IR spectroscopy enables the measure of other structure parameters as the relative orientation of vibrational transition dipole moments in molecules such as peptides [9–12], and their fluctuations in equilibrium with a

subpicosecond time resolution. [10,13–17] The time delay between the IR_{pump} and IR_{probe} pulses is typically chosen between few hundred femtoseconds (fs) up to several picoseconds (ps). Therefore the high time resolution of less than 1 ps is the most promising potential of 2D IR spectroscopy. 2D IR spectroscopy allows the observation of chemical exchange process in real time as most of the molecular dynamics freeze in such a "snapshot". [18] Therefore, the high time resolution helps to distinguish between dynamically coupled subconformations in equilibrium states. [19]

Transient two-dimensional infrared (T2D IR) spectroscopy describes the extension of 2D IR spectroscopy studying systems at equilibrium to the observation of nonequilibrium systems. For that reason, an ultraviolet (UV) or visible laser pulse triggers an reaction, for example a photo reaction, and subsequently, the 2D IR snapshot is taken of the nonequilibrium ensemble. Photo reactions as well as other reactions of a nonequilibrium system appear on a picosecond timescale such that T2D IR spectroscopy takes full advantage of the high time resolution as it allows the investigation of transient species. [4,20] Fig. 1(b) shows the T2D IR spectrum of the Rhenium-complex. Besides the peaks, which have already observed in the 2D IR spectrum, new peaks appear. These peaks are frequency shifted along the diagonal. The frequency shift is induced by the photo excitation of the UV_{pump} pulse. [21–23] Therefore T2D IR spectroscopy leads to new insights [4,20,24,25] since T2D IR spectroscopy correlates ground and excited state vibrations.

The main subject of this thesis is to introduce a T2D IR spectroscopy setup. This setup has been designed to provide 2D spectra with high temporal and spectral resolution on the one hand and on the other hand it was taken care of that the experimental handling is simple and the measurement time is short. The presented 2D and T2D IR spectra in Fig. 1 are measured simultaneously within 10 minutes using the T2D IR spectroscopy setup.

2 Nonlinear response theory

Nonlinear response theory provides a mathematical description of nonlinear spectroscopy. The following derivation is based on the treatments of S. Mukamel [26] and P. Hamm [27] and is meant to give a simple introduction. Additional information and a more detailed derivation can be found in Refs. [26, 27].

Nonlinear response theory describes the interaction of light with matter and uses the perturbative expansion of the polarization (Section 2.4). The polarization is calculated quantum mechanically using the density matrix formalism and its perturbative expansion, which therefore needs to be introduced first, (Section 2.1 and 2.3).

In spectroscopy the Hamiltonian describing the system is typically divided into a time-dependent and time-independent part such that the interaction picture is usually applied to simplify the derivation of the response functions (Section 2.2). Eventually, the response functions are derived (Section 2.5) which contain all information about a material that can be measured with nonlinear spectroscopy of a given order.

2.1 The density matrix

The density matrix of a pure quantum state[1] in a basis-free representation is defined as:

$$\rho \equiv |\varphi\rangle \langle\varphi| \tag{1}$$

However, in general one rather has to consider a statistical ensemble of molecules. Furthermore, one cannot define a wavefunction of a statistical average. If one considers the probability p_s of a system to be in a state $|\varphi_s\rangle$, the mixed density matrix of the ensemble is defined as a linear superposition of the different pure states $|\varphi_s\rangle$:

$$\rho = \sum_s p_s |\varphi_s\rangle \langle\varphi_s| \ , \tag{2}$$

with $p_s \geq 0$ and $\sum_s p_s = 1$ (normalization).
The time evolution of a density matrix can be determined using the time-dependent Schrödinger equation:

$$\frac{\partial}{\partial t} |\varphi(t)\rangle = -\frac{i}{\hbar} \hat{H}(t) |\varphi(t)\rangle \tag{3}$$

and is denoted as the Liouville-von Neumann equation:

$$\frac{\partial}{\partial t}\rho = -\frac{i}{h} \left[\hat{H}, \rho\right] . \tag{4}$$

[1] A quantum-mechanical state of a single molecule that can be described by a single wavefunction φ is called a pure state.

The expectation value of an operator $\hat{A}$ is defined as $\langle\hat{A}\rangle \equiv \langle\varphi|\hat{A}|\varphi\rangle$ such that using the density matrix yields:

$$\langle\hat{A}\rangle = \mathrm{Tr}(\rho \cdot \hat{A}) \equiv \langle\rho \cdot \hat{A}\rangle. \tag{5}$$

2.2 Interaction picture

The interaction picture is useful since it facilitates the separation of a Hamiltonian into time-dependent and time-independent terms which simplifies the derivation of the response functions. In spectroscopy, it is common to write the system Hamiltonian $\hat{H}$ as the sum of a time-independent and a time-dependent term:

$$\hat{H}(t) = \hat{H}_0 + \hat{V}(t) \tag{6}$$

The time-independent term $\hat{H}_0$ describes the molecular Hamiltonian with no interaction between the applied electric field and the molecules. The time-dependent term $\hat{V}(t)$ is usually much weaker and describes the interaction of the molecules with the time-dependent electric field:

$$\hat{V}(t) = -\hat{\mu} \cdot E(t). \tag{7}$$

The time evolution operator is defined with respect to the time-independent system Hamiltonian $\hat{H}_0$ as follows:

$$\hat{U_0}(t, t_0) = e^{-\frac{i}{\hbar}\hat{H}_0 \cdot (t - t_0)}, \tag{8}$$

such that the wavefunction in the interaction picture is defined as

$$|\varphi(t)\rangle \equiv \hat{U_0}(t, t_0)\,|\varphi_I(t)\rangle\,, \tag{9}$$

the subscript I denotes the interaction picture. Introducing Eq. 9 into the Schrödinger equation (Eq. 3) one obtains

$$\frac{\partial}{\partial t}\,|\varphi_I(t)\rangle = -\frac{i}{\hbar}\hat{V}_I(t)\,|\varphi_I(t)\rangle \tag{10}$$

with

$$\hat{V}_I(t) = e^{-\frac{i}{\hbar}\hat{H}_0 \cdot (t - t_0)}\hat{V}(t)e^{+\frac{i}{\hbar}\hat{H}_0 \cdot (t - t_0)}, \tag{11}$$

the definition of the weak perturbation $\hat{V}_I(t)$ in the interaction picture. Eq. 10 is formally equivalent to the Schrödinger equation (Eq. 3) in the Schrödinger picture.

2.3 Perturbative expansion of the density matrix

The definition of the wavefunction in the interaction picture (Eq. 9) leads to the following definition of the density matrix for the interaction picture:

$$|\varphi(t)\rangle \langle\varphi(t)| = e^{-\frac{i}{\hbar}\hat{H}_0\cdot(t-t_0)} |\varphi_I(t)\rangle \langle\varphi_I(t)| e^{+\frac{i}{\hbar}\hat{H}_0\cdot(t-t_0)} \tag{12}$$

or

$$\rho(t) = e^{-\frac{i}{\hbar}\hat{H}_0\cdot(t-t_0)}\rho_I(t)e^{+\frac{i}{\hbar}\hat{H}_0\cdot(t-t_0)}. \tag{13}$$

The time evolution of the density matrix in the interaction picture using Eq. 10 yields:

$$\frac{\partial}{\partial t}\rho_I(t) = -\frac{i}{\hbar}\left[\hat{V}_I(t), \rho_I(t)\right] \tag{14}$$

which is formally equivalent to the Liouville-von Neumann equation (Eq. 4).
The perturbative expansion of the density matrix is derived by formally integrating Eq. 14

$$\rho_I(t) - \rho_I(t_0) = -\frac{i}{\hbar}\int_{t_0}^{t} dt \left[\hat{V}_I(\tau), \rho_I(\tau)\right] \tag{15}$$

and then solve the resulting Eq. 15 iteratively by plugging it into itself:

$$\begin{aligned}\rho_I(t) &= \rho_I(t_0) + \left(-\frac{i}{\hbar}\right)\int_{t_0}^{t} d\tau_1 \left[\hat{V}_I(\tau_1), \rho(t_0)\right] + \\ &+ \left(-\frac{i}{\hbar}\right)^2 \int_{t_0}^{t} d\tau_2 \int_{t_0}^{\tau_2} d\tau_1 \left[\hat{V}_I(\tau_2), \left[\hat{V}_I(\tau_1), \rho_I(t_0)\right]\right] ...\end{aligned} \tag{16}$$

and after n iterations one obtains:

$$\begin{aligned}\rho_I(t) &= \rho_I(t_0) + \sum_{n=1}^{\infty}\left(-\frac{i}{\hbar}\right)^n \int_{t_0}^{t} d\tau_n \int_{t_0}^{\tau_n} d\tau_{n-1} ... \int_{t_0}^{\tau_2} d\tau_1 ... \\ &\left[\hat{V}_I(\tau_n), \left[\hat{V}_I(\tau_{n-1}), ... \left[\hat{V}_I(\tau_1), \rho_I(t_0)\right]\right]\right].\end{aligned} \tag{17}$$

The perturbative expansion of the density matrix can be written in the Schrödinger picture using the time evolution operator (Eq. 8):

$$\begin{aligned}\rho(t) &= \rho^{(0)}(t_0) + \sum_{n=1}^{\infty}\left(-\frac{i}{\hbar}\right)^n \int_{t_0}^{t} d\tau_n \int_{t_0}^{\tau_n} d\tau_{n-1} ... \int_{t_0}^{\tau_2} d\tau_1 ... \\ &e^{-\frac{i}{\hbar}\hat{H}_0\cdot(t-t_0)} \left[\hat{V}_I(\tau_n), \left[\hat{V}_I(\tau_{n-1}), ... \left[\hat{V}_I(\tau_1), \rho_I(t_0)\right] ...\right]\right] e^{+\frac{i}{\hbar}\hat{H}_0\cdot(t-t_0)},\end{aligned} \tag{18}$$

such that

$$\rho(t) \equiv \rho^{(0)}(t) + \sum_{n=1}^{\infty}\rho^{(n)}(t), \tag{19}$$

where $\rho^{(0)}$ is the 0^{th}-order density matrix[2] and the n^{th}-order density matrices $\rho^{(n)}$ are ordered in powers of $\hat{V}_I$ which are in the interaction picture and contain both the perturbation $\hat{V}_I(t)$ and time evolution operators.[3]

The perturbation term $V(t)$ describes the interaction of the system with the electric field (Eq. 7) such that the n^{th}-order density is (ignoring polarization)

$$\begin{aligned}\rho^{(n)}(t) &= -\left(-\frac{i}{\hbar}\right)^n \int_{t_0}^{t} d\tau_n \int_{t_0}^{\tau_n} d\tau_{n-1} ... \int_{t_0}^{\tau_2} d\tau_1 E(\tau_n)\cdot E(\tau_{n-1})\cdot ...\cdot E(\tau_1)\cdot \\ & e^{-\frac{i}{\hbar}\hat{H}_0\cdot(t-t_0)}\left[\hat{\mu}_I(\tau_n),[\hat{\mu}_I(\tau_{n-1}),...\left[\hat{\mu}_I(\tau_1),\rho(t_0)\right]...\right]\right] e^{+\frac{i}{\hbar}\hat{H}_0\cdot(t-t_0)} \qquad (20)\end{aligned}$$

with the following definition of the dipole operator in the interaction picture:

$$\hat{\mu}_I(t) = e^{+\frac{i}{\hbar}\hat{H}_0\cdot(t-t_0)}\hat{\mu}e^{-\frac{i}{\hbar}\hat{H}_0\cdot(t-t_0)}.^4 \qquad (21)$$

2.4 Perturbative expansion of the polarization

An electromagnetic field interacting with a matter generates a polarization in the matter. In linear optics, the electric field is weak such that only effects emerge which are linearly proportional to the strength of the incident electric field. The interaction between electric field and matter are characterized by the dielectric susceptibility tensor χ:

$$P_j(t) = \varepsilon_0 \cdot \chi_{ji} \cdot E^i(t), \qquad (22)$$

where $P(t)$ is the macroscopic polarization in the matter as response to the applied electric field $E(t)$ and ε_0 is the absolute dielectric constant in vacuum ($\varepsilon_0 = \frac{1}{\mu_0 c_0^2}\ \frac{\mathrm{F}}{\mathrm{m}}$).

For strong incident electric fields, as generated by lasers, nonlinear effects emerge. Thus Eq. 22 is no longer valid and the polarization has to be expanded in powers of the electric field $E(t)$:

$$\begin{aligned}P_m(t) &= \varepsilon_0 \left(\chi^{(1)}_{mi}\cdot E^i(t) + \chi^{(2)}_{mij}\cdot E^i(t)\cdot E^j(t) + \chi^{(3)}_{mijk}\cdot E^i(t)\cdot E^j(t)\cdot E^k(t) + ...\right) \qquad (23)\\ &= P^{(1)}(t) + P^{(2)}(t) + P^{(3)}(t) + ... \qquad (24)\end{aligned}$$

The polarization $P(t)$ can be written as a combination of a linear and nonlinear term:

$$P(t) = P_L(t) + P_{NL}(t) \qquad (25)$$

[2] 0^{th}-order describes the evolution of the system as there was no perturbation.

[3] The perturbative terms describe the effect of the interaction with the electrical field and have an intuitive physical interpretation: The system propagates freely under subject of the system Hamiltonian $\hat{H}_0$ until time τ_1, described by the time evolution operator $e^{-\frac{i}{\hbar}\hat{H}_0(\tau_1-t_0)}$. At time τ_1, it interacts with the perturbation $\hat{V}(\tau_1)$. Subsequently, it again propagates freely until time τ_2, and so on. [27]

[4] The subscript I is not necessary since dipole operators are only time-dependent in the interaction picture and not in the Schrödinger picture such that it is automatically clear what picture the dipole operators are in.

with

$$P_L = P^{(1)} = \varepsilon_0 \chi^{(1)}_{mi} E^i(t) \tag{26}$$

and

$$P_{NL} = P^{(2)} + P^{(3)} + ... = \varepsilon_0 \left(\chi^{(2)}_{mij} \cdot E^i(t) \cdot E^j(t) + \chi^{(3)}_{mijk} \cdot E^i(t) \cdot E^j(t) \cdot E^k(t) + ... \right). \tag{27}$$

$\chi^{(1)}$ is the first-order (linear) susceptibility and $\chi^{(n)}$ ($n \geq 2$) the n^{th}-order (nonlinear) susceptibility tensor. The linear polarization, $P_L(t)$ describes physical processes such as the absorption and refraction of light. $P^{(2)}(t)$ characterizes three-wave mixing processes[5], such as sum frequency generation (SFG), and difference frequency generation (DFG); $P^{(3)}(t)$ is responsible for four-wave mixing processes, such as two-photon absorption, self-phase modulation, and, of course, the pump-probe response.

The macroscopic polarization is given by the expectation value of the dipole operator $\hat{\mu}$:

$$P(t) = \langle \hat{\mu} \rangle = \mathrm{Tr}(\hat{\mu}\rho(t)) \equiv \langle \hat{\mu}\rho(t) \rangle . \tag{28}$$

Expanding the polarization in powers of the electric field $E(t)$ and substituting the density matrix in Eq. 28 by its perturbative expansion yields

$$P(t) = \left\langle \hat{\mu} \left(\rho^{(0)}(t) + \rho^{(1)} + \rho^{(2)} + ... \right) \right\rangle , \tag{29}$$

such that the n^{th}-order polarization is

$$P^{(n)}(t) = \left\langle \hat{\mu} \cdot \rho^{(n)} \right\rangle . \tag{30}$$

2.5 Response functions

The macroscopic polarization is given by the expectation value of the dipole operator $\hat{\mu}$ such that one obtains the nth-order polarization

$$\begin{aligned} P^{(n)} &= -\left(-\frac{i}{\hbar}\right)^n \int_{t_0}^{t} d\tau_n \int_{t_0}^{\tau_n} d\tau_{n-1} \, ... \int_{t_0}^{\tau_2} d\tau_1 \; E(\tau_n) \cdot \\ & \quad E(\tau_{n-1}) \cdot ... \cdot E(\tau_1) \cdot \langle \hat{\mu}(t) \left[\hat{\mu}(\tau_n), ... \left[\hat{\mu}(\tau_1), \rho(t_0) \right] ... \right] \rangle \end{aligned} \tag{31}$$

from Eq. 20, Eq. 28, and Eq. 30.

[5] n^{th}-order polarization describes $(n+1)$-wave mixing processes which involve the interaction of n electric fields with wave vectors $\vec{k}_1, \vec{k}_2, ..., \vec{k}_n$ and frequencies $\omega_1, \omega_2, ..., \omega_n$, respectively, with the material system. [26]

The nth-order nonlinear polarization can be written as a convolution of n electric fields

$$P^{(n)} = -\left(-\frac{i}{\hbar}\right)^n \int_{t_0}^{t} d\tau_n \int_{t_0}^{\tau_n} d\tau_{n-1} \ldots \int_{t_0}^{\tau_2} d\tau_1 \; E(\tau_n) \cdot E(\tau_{n-1}) \cdot \ldots$$
$$\cdot E(\tau_1) \cdot R^{(n)}(t-\tau_n, \tau_n - \tau_{n-1}, ..., \tau_2 - \tau_1) \tag{32}$$

with the n^{th}-order response function:

$$R^{(n)}(t-\tau_n, \tau_n - \tau_{n-1}, ..., \tau_2 - \tau_1) = \left(-\frac{i}{\hbar}\right)^n \langle \hat{\mu}(t) \left[\hat{\mu}(\tau_n), \ldots \left[\hat{\mu}(\tau_1), \rho(-\infty)\right] \ldots\right]\rangle \,. \tag{33}$$

In nonlinear spectroscopy with short pulses the order of interactions with the different fields is known and one can assume that the integral is time-ordered ($\tau_1 \leq \tau_2 \leq \ldots \leq t$) and choose the arbitrary zero-point at τ_1. Furthermore, since $R^{(n)}$ only depends on the time intervals it is common to use the time intervals t instead of the absolute time points τ:

$$\begin{aligned} \tau_1 &= 0 \\ t_1 &= \tau_2 - \tau_1 \\ t_2 &= \tau_3 - \tau_2 \\ &\vdots \\ t_n &= t - \tau_n, \end{aligned}$$

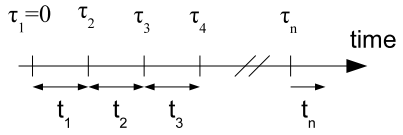

Figure 2: Time variable transformation: τ's refer to the absolute time points and t's to the time intervals.

This time variable transformation is illustrated in Fig. 2. In terms of these variables the nth-order polarization reads

$$P^{(n)} = -\left(-\frac{i}{\hbar}\right)^n \int_0^{\infty} dt_n \int_0^{\infty} dt_{n-1} \ldots \int_0^{\infty} dt_1 E(t-t_n) \cdot E(t-t_n-t_{n-1}) \cdot \ldots$$
$$\cdot E(t-t_n-\ldots-t_1) \cdot R^{(n)}(t_n, t_{n-1}, ..., t_1) \tag{34}$$

with

$$R^{(n)}(t_n, ..., t_1) = \left(-\frac{i}{\hbar}\right)^n \langle \hat{\mu}(t_n + \ldots + t_1) \left[\hat{\mu}(t_{n-1} + \ldots + t_1), \ldots \left[\hat{\mu}(0), \rho(-\infty)\right] \ldots\right]\rangle \,. \tag{35}$$

The nth-order response function calculated explicitly yields 2^n terms with various numbers of dipole operators acting either on the left (i.e. on the ket) or on the right (i.e. on the bra) of the density matrix. For higher orders, the single terms of the response function become long, complex and are no longer intuitive. However, a simple way to graphically describe the terms has been devised. Each of these terms can be illustrated by a Feynman diagram if the following rules are followed: [26, 27]

1. The left and right vertical line represent the time evolution of the ket $|...\rangle$ and bra $\langle ...|$ of the density matrix. Time runs from bottom to top.
2. Interactions with the light field are represented by arrows. The last interaction, which originates from the trace $P^{(n)}(t) = \left\langle \hat{\mu}(t)\rho^{(n)}(t)\right\rangle$, is emission and hence indicated using a different arrow.
3. Each diagram has a sign $(-1)^n$, where n is the number of interactions from the right.
5. An arrow pointing towards the system represents an up-climbing of bra or ket of the density matrix, while an arrow pointing away represents a de-excitation.
4. An arrow pointing to the right represents an electric field with $e^{-i\omega t+i\vec{k}\cdot\vec{r}+i\phi}$, while an arrow pointing to the left represents an electric field with $e^{+i\omega t-i\vec{k}\cdot\vec{r}-i\phi}$. This rule expresses the fact that the real electric field

   $$E(t) = 2E'(t)\cdot\cos(\omega t - \vec{k}\cdot\vec{r} - \phi)$$

   can be separated into positive and negative frequencies

   $$E(t) = E'(t)\cdot\left(e^{-i\omega t+i\vec{k}\cdot\vec{r}+i\phi} + e^{+i\omega t-i\vec{k}\cdot\vec{r}-i\phi}\right).$$

   The emitted light, i.e. the last interaction, has a frequency and a wavevector which is the sum of the input frequencies and wavevectors (considering the appropriate signs).
6. The last interaction must end in a population state.

Each Feynman diagram describes one term of the response function such that the Feynman diagrams give an intuitive illustration of the process for each term of the response function. The linear (1^{st}-order) response function is the simplest and according to Eq. 35 it is

$$R^{(1)}(t_1) = -\frac{i}{\hbar}\cdot\langle\hat{\mu}(t-1)\,[\hat{\mu}(0),\rho(-\infty)]\rangle \tag{36}$$

$$= -\frac{i}{\hbar}\cdot\left(\langle\hat{\mu}(t_1)\hat{\mu}(0)\rho(-\infty)\rangle - \langle\hat{\mu}(t_1)\rho(-\infty)\hat{\mu}(0)\rangle\right), \tag{37}$$

which can be written as[6]:

$$R^{(1)} = -\frac{i}{\hbar}\left(\langle\mu(t_1)\mu(0)\rho(-\infty)\rangle - \langle\mu(t_1)\mu(0)\rho(-\infty)\rangle^{\dagger}\right). \tag{39}$$

Eq. 39 shows mathematically that the second term is the conjugate complex of the first. The two Feynman diagrams of the linear response functions are presented in Fig. 3

[6]Use the invariance of the trace $\langle ...\rangle$ on cyclic permutation and, since all operators are Hermitian, the following equivalence holds:

$$\left\langle(\hat{\mu}(t_1)\hat{\mu}(0)\rho(-\infty))^{\dagger}\right\rangle = \left\langle\rho^{\dagger}(-\infty)\hat{\mu}^{\dagger}(0)\hat{\mu}^{\dagger}(t_1)\right\rangle = \langle\rho(-\infty)\hat{\mu}(0)\hat{\mu}(t_1)\rangle \tag{38}$$

which shows that the conjugate complex diagrams is the mirror image of the other. By convention, only the Feynman diagrams with the emission arrow pointing to the left are drawn.

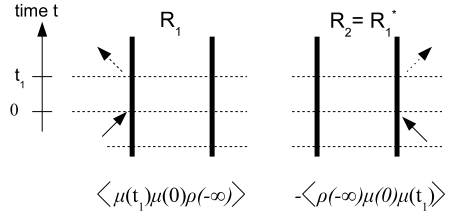

Figure 3: Feynman diagrams of the linear response. Right Feynman diagram is the conjugate complex of the left. $R_1 = \langle\mu(t_1)\mu(0)\rho(-\infty)\rangle$ and $R_2 = R_1^* = -\langle\mu(t_1)\rho(-\infty)\mu(0)\rangle$. The vertical left line denotes the time evolution of the ket of the density matrix and the right line of the bra.

The 3^{rd}-order response function is the relevant case for nonlinear spectroscopy considered here and one can derive: [26]

$$
\begin{aligned}
R^{(3)} &= \langle\hat{\mu}(t_3+t_2+t_1)\,[\hat{\mu}(t_2+t_1),[\hat{\mu}(t_1),[\hat{\mu}(0),\rho(-\infty)]]]\rangle \qquad (40)\\
&= \langle\hat{\mu}(t_3+t_2+t_1)\hat{\mu}(t_1)\rho(-\infty)\hat{\mu}(0)\hat{\mu}(t_2+t_1)\rangle \quad \Rightarrow \quad R_1\\
&+ \langle\hat{\mu}(t_3+t_2+t_1)\hat{\mu}(t_2+t_1)\rho(-\infty)\hat{\mu}(0)\hat{\mu}(t_1)\rangle \quad \Rightarrow \quad R_2\\
&+ \langle\hat{\mu}(t_3+t_2+t_1)\hat{\mu}(0)\rho(-\infty)\hat{\mu}(t_1)\hat{\mu}(t_2+t_1)\rangle \quad \Rightarrow \quad R_3\\
&+ \langle\hat{\mu}(t_3+t_2+t_1)\hat{\mu}(t_2+t_1)\hat{\mu}(t_1)\hat{\mu}(0)\rho(-\infty)\rangle \quad \Rightarrow \quad R_4\\
&- \langle\hat{\mu}(t_3+t_2+t_1)\hat{\mu}(t_2+t_1)\hat{\mu}(0)\rho(-\infty)\hat{\mu}(t_1)\rangle \quad \Rightarrow \quad R_5 = R_1^*\\
&- \langle\hat{\mu}(t_3+t_2+t_1)\hat{\mu}(t_1)\hat{\mu}(0)\rho(-\infty)\hat{\mu}(t_2+t_1)\rangle \quad \Rightarrow \quad R_6 = R_2^*\\
&- \langle\hat{\mu}(t_3+t_2+t_1)\hat{\mu}(t_2+t_1)\hat{\mu}(t_1)\rho(-\infty)\hat{\mu}(0)\rangle \quad \Rightarrow \quad R_7 = R_3^*\\
&- \langle\hat{\mu}(t_3+t_2+t_1)\rho(-\infty)\hat{\mu}(0)\hat{\mu}(t_1)\hat{\mu}(t_2+t_1)\rangle \quad \Rightarrow \quad R_8 = R_4^*
\end{aligned}
$$

and the corresponding Feynman diagrams are shown in Fig. 4.

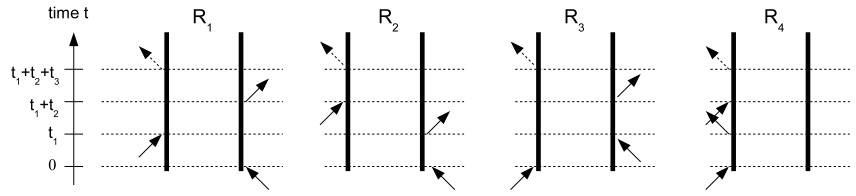

Figure 4: Feynman diagrams of the 3^{rd}-order response function. Feynman diagrams $R_5 - R_8$, which represent the conjugate complex of the Feynman diagrams $R_1 - R_4$, are not drawn.

3 Phenomenological description of 2D IR spectroscopy

The flagship of 2D IR spectroscopy and the resulting 2D IR spectra are the so-called cross-peaks between two coupled oscillators. [10,28] Nevertheless, a 2D IR spectrum of a single oscillator is introduced first to describe the basic principles. In the second part of this section, the appearance of the cross-peaks in a 2D IR spectrum is discussed based on two coupled oscillators.

3.1 2D IR spectrum of a single oscillator

To facilitate the discussion, one considers a pump-probe experiment to generate a 2D IR spectrum. A three-level scheme of an anharmonic oscillator is regarded as shown in Fig. 5.
At thermal equilibrium, all molecules are assumed to be in the ground state $|0\rangle$. Then an IR pump pulse excites a certain fraction of molecules from ground state $|0\rangle$ to the first excited state $|1\rangle$, Fig. 5(a). The subsequent probe pulse acts now on the nonequilibrium system and causes three transitions, labeled 1, 2, and 3 in Fig. 5(b). The transition (1) and (2) originate from the excited state $|1\rangle$: (1) describes the excited state absorption to the second excited state $|2\rangle$, and (2) is the stimulated emission back to the ground state $|0\rangle$. The third transition (3) describes the possible excitation from ground state $|0\rangle$ to the first excited state $|1\rangle$ of previously unexcited molecules. Due to the prior pump pulse a smaller fraction can now be excited. The $|0\rangle \rightarrow |1\rangle$ transition (3), after a preceding excitation, is called a bleach.

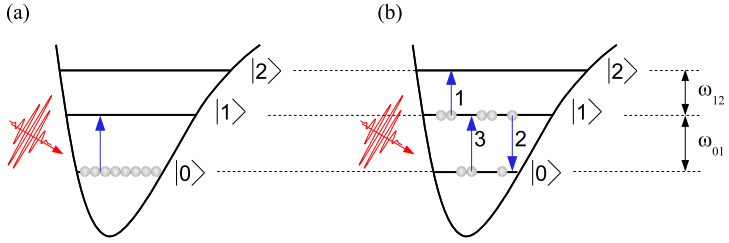

Figure 5: Principle of pump-probe spectroscopy on a three-level scheme of an anharmonic oscillator. (a) In thermal equilibrium all molecules are in the ground state $|0\rangle$. A pump pulse promotes a significant fraction of the molecules to the first excited state $|1\rangle$. (b) The probe pulse causes three interactions: (1) excited state absorption, (2) stimulated emission, and (3) bleach.

Fig. 6 illustrates the one-dimensional (1D) absorbance spectra. One typically normalizes the transmitted light I with the light I_0 in front of the sample and the absorption is described by Lambert-Beer's law:

$$A = -\log_{10}\left(\frac{I}{I_0}\right). \tag{41}$$

By convention a 1D pump-probe absorbance spectrum describes the difference spectrum of 1D spectra with and without preceding pump pulse. Therefore the difference absorbance spectrum ΔA is

$$\Delta A = A_{\text{unpumped}} - A_{\text{pumped}} \tag{42}$$

$$= -\log_{10}\left(\frac{I_{\text{unpumped}}}{I_0}\right) - \left(-\log_{10}\left(\frac{I_{\text{pumped}}}{I_0}\right)\right) \tag{43}$$

$$\Delta A = -\log_{10}\left(\frac{I_{\text{pumped}}}{I_{\text{unpumped}}}\right) \tag{44}$$

which is graphically described in Fig. 6.
If the system experienced no pump pulse excitation, the probe pulse will act on the system being in thermal equilibrium. Thus, the probe pulse causes only the $|0\rangle \rightarrow |1\rangle$ transition and in the 1D absorption spectra a peak will arise at transition frequency ω_{01}, Fig. 6(a). Whereas the probe pulse after preceding pump pulse causes three transitions, Fig. 5(b). The molecules can absorb light at frequency ω_{12} and excite to $|2\rangle$ giving rise to a small peak at transition frequency ω_{12}, Fig. 6(b). This frequency shift to lower frequencies is due to the anharmonic potential of the oscillator which concludes in $\omega_{12} < \omega_{01}$. Also a peak appears at transition frequency ω_{01} due to stimulated emission and bleach. The peaks in this 1D absorbance spectrum are smaller since the molecules are distributed to state $|1\rangle$ and $|2\rangle$. Eventually, Fig. 6(c) shows the difference spectra which results in two peaks with different signs, the light absorption appears positive.

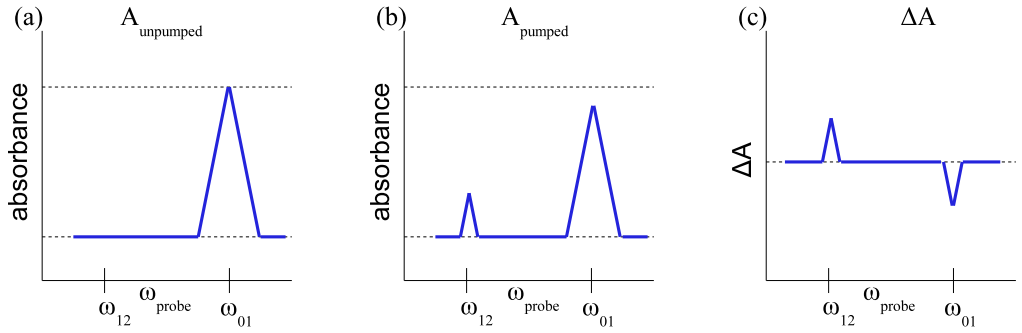

Figure 6: Principle of an one-dimensional difference absorption spectrum. (a) An absorbance spectrum of a single oscillator without preceding pump pulse. Light is only absorbed by the molecules in the ground state. (b) The preceding pump pulse promotes a significant fraction of the molecules to the first excited state. The $|0\rangle \rightarrow |1\rangle$ transitions and the excited state absorption $|1\rangle \rightarrow |2\rangle$ lead to the peaks at ω_{01} and ω_{12}. (c) The difference spectrum of probe absorption where two peaks appear with different signs. The positive peak denotes light absorption and the negative peak light emission.

In the end, the 2D IR spectrum is a plot of the absorption as a function of the pump and probe frequencies. One observes a doublet of peaks with opposite signs (Fig. 7(b))

according to the 1D absorbance spectra, Fig. 6(c). The on-diagonal peak at $\omega_{\text{pump}} = \omega_{\text{probe}} = \omega_{01}$ occurs due to the stimulated emission (2) and the bleach (3) signals. The excited state absorption (1) signal appears with a peak at $\omega_{\text{pump}} = \omega_{01}$ and $\omega_{\text{probe}} = \omega_{12}$. These two peaks describe an on-diagonal peak doublet.

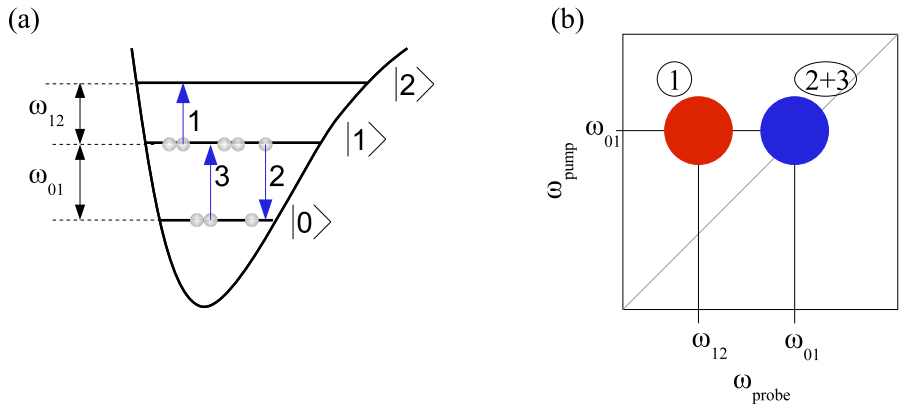

Figure 7: (a) Three-level scheme of a single oscillator. (b) On-diagonal peak doublet appears in the 2D IR spectrum. The peaks are caused by the transition labeled with the same numbers in the three-level scheme.

3.2 2D IR spectrum of two coupled oscillators

If two oscillators are coupled then the excitation of one oscillator causes a change of the frequency of the second oscillator and off-diagonal peak doublets, the so called cross-peaks, appear.
Two coupled oscillators have a common ground state and a combination band as illustrated in the corresponding three-level scheme in Fig. 8(a). The principle of the 2D IR spectrum in Fig. 8(b) can be described using the three-level scheme. Each arrow in the level scheme, Fig. 8(a), marks an allowed transition which is responsible for a peak in the resulting 2D IR spectrum. One observes on-diagonal and off-diagonal peak doublets where the on-diagonal doublets only involve one oscillator and the off-diagonal doublets involve two oscillators.

A simple pump-probe picture with the pump beam being in resonance with, for example, the first oscillator (#1) at frequency ω_1 can explain the 2D IR spectrum of two coupled oscillators. The pump beam will excite some of the molecules from the common ground state $|00\rangle$[7] to $|10\rangle$, the first excited state of oscillator #1. The subsequent probe beam can now induce the transitions (1),(2),(3),(5), and (7) depicted by the labeled arrows in Fig. 8(a).

[7]Nomenclature for labeling the eigenstates of two coupled oscillators: $|kl\rangle$ describes a state with k quanta of excitation in the first mode and l quanta of excitation in the second mode. [27]

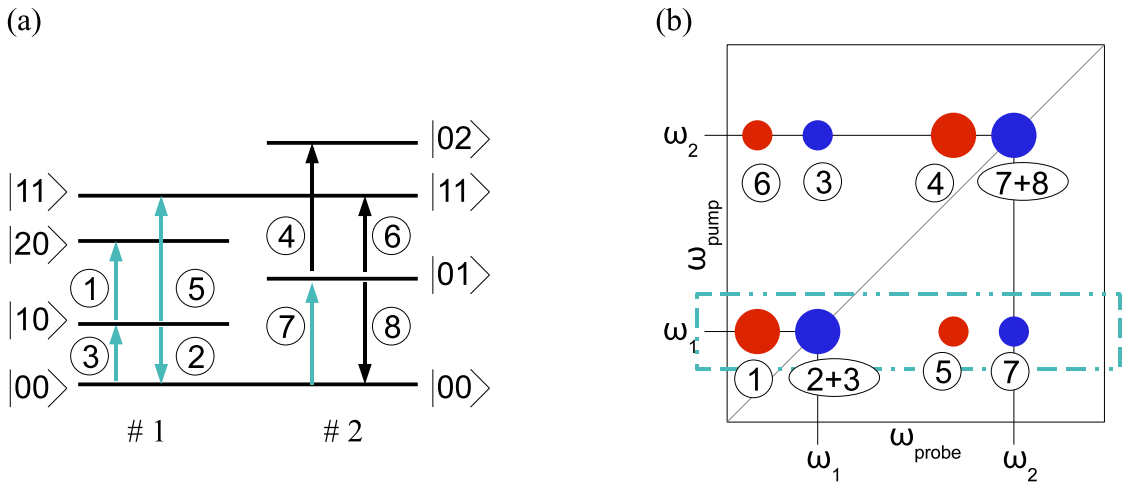

Figure 8: (a) Level scheme of two coupled oscillators. $|kl\rangle$ denotes a state with k quanta in the first oscillator #1 and l quanta in the second oscillator #2. The dipole-allowed transitions are depicted. The cyan colored arrows mark the transitions discussed in the text. (b) Schematical 2D IR spectrum. Blue peaks present negative response (bleach and stimulated emission), red peaks positive response (excited state absorption). The labels (1) to (8) relate each peak to the corresponding transition in the level scheme. The cyan dashed box marks the peaks discussed in the text.

Arrows (1),(2), and (3) show the same transitions as discussed for a single oscillator generating the on-diagonal peak doublet and these transition do not contribute to the off-diagonal peak doublet (the cross-peak). The off-diagonal peak (5) corresponds to the $|10\rangle \rightarrow |11\rangle$ absorption while peak (7) corresponds to the $|00\rangle \rightarrow |01\rangle$ bleach. If the two oscillators are not coupled the excitation of the second oscillator (#2), from $|...0\rangle$ to $|...1\rangle$, would not care about the excitation level of the first. Consequently, the frequencies $\omega_{|10\rangle\rightarrow|11\rangle}$ and $\omega_{|00\rangle\rightarrow|01\rangle}$ are equal, such that the peaks (5) and (7) coincide and cancel each other due to the identical transition strength but opposite signs of both contributions. Hence, no cross-peaks appear for uncoupled oscillators. [27]
Thus, the existence of a cross-peak in a 2D IR spectrum is a direct manifestation of the coupling between two oscillators meaning that the transition frequency of one oscillator depends on the excitation level of the other. In that sense, the existence of cross-peaks is related to molecular structure information. [10, 27, 28]

4 Spectroscopy described by response theory

The concept of molecules and their population in different quantum states suits well to give an intuitive description of 2D IR spectroscopy and the resulting 2D IR spectra (Section 3). However, to discuss different 2D IR spectroscopy methods an explanation based on electromagnetic (e.m.) fields is more convenient, using the response theory introduced in Section 2 for description.

1^{st}-order linear spectroscopy
Linear absorption is the simplest spectroscopy case and therefore useful to get an basic understanding before discussing the 3^{rd}-order nonlinear spectroscopy concept.

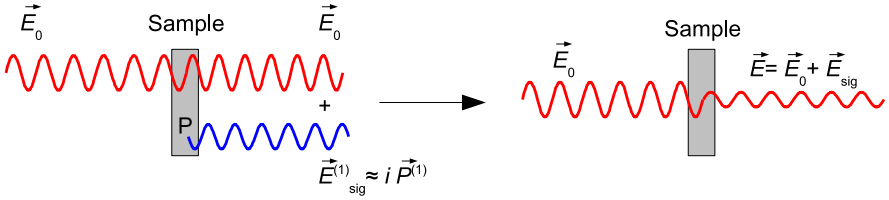

Figure 9: An electromagnetic (e.m.) wave induces an oscillating polarization in a material. The polarization radiates a secondary e.m. wave $\vec{E}_{\text{sig}}$ which is out of phase with the original wave $\vec{E}_0$. Therefore the two waves interfere destructively which is a way of expressing the absorption of the radiation by the material.

An e.m. wave $\vec{E}_0$ interacts on a material in which it induces an oscillating polarization $\vec{P}$. According to Maxwell's equation, the macroscopic polarization radiates a new e.m. wave $\vec{E}_{\text{sig}}$ that runs out of phase with the original wave $\vec{E}_0$, Fig. 9. The 90° phase shift of the emitted field relative to the polarization can be written as: [26]

$$E^{(1)}_{\text{sig}}(t) \propto i \cdot P^{(1)}(t) \tag{45}$$

The induced polarization depends linearly on the incident light field as derived in Eq. 31:

$$P^{(1)}(t) = \frac{i}{\hbar} \int_0^\infty dt_1 \; E_0(t - t_1) \cdot R^{(1)}(t_1) \tag{46}$$

with linear response function $R^{(1)}$. The simplest example is described by a two-level system, Fig. 10(a) and only one Feynman diagram (Fig. 10(b)) exists for the response function $R^{(1)}$. The system is assumed to be in thermal equilibrium, ground state $|0\rangle\langle 0|$, before an e.m. wave $\vec{E}_0$ interacts with the system. Upon interaction with the laser pulse a coherence state $|1\rangle\langle 0|$ is generated which then radiates a 1^{st}-order polarization $P^{(1)}(t)$ depicted by the dotted arrow. The rules given for the Feynman diagrams (Section 2.5) imply that the emitted field $P^{(1)}(t)$ is radiated in the same direction $\vec{k}$ given by the incident field of the single laser pulse. Hence, the incident field and the emitted field interfere destructively, which expresses the absorption of light and one says that the emitted field is heterodyned by $\vec{E}_0$.

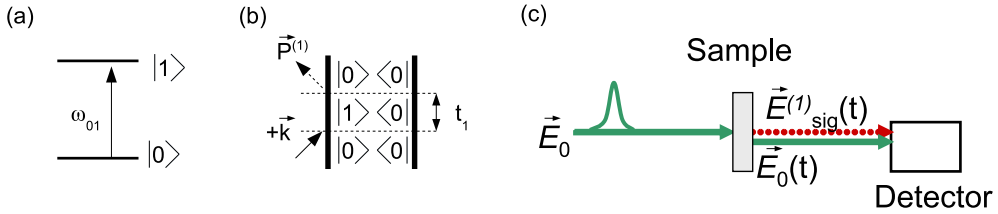

Figure 10: (a) Scheme of a two-level system as simplest example for linear absorption. (b) The only existing Feynman diagram of the resulting response function $R^{(1)}$ for linear absorption. (c) Schematical description of a linear absorption experiment.

3^{rd}-order nonlinear spectroscopy

In 3^{rd}-order nonlinear spectroscopy two or three laser beams are directed onto the sample and the laser fields interact three times with the molecular system. The induced polarization is described by Eq. 31:

$$P^{(3)}(t) = -\frac{i}{\hbar^3}\int_0^\infty dt_3 \int_0^\infty dt_2 \int_0^\infty dt_1 \; E_3(t-t_3)\cdot E_2(t-t_3-t_2)\cdot E_1(t-t_3-t_2-t_1)\cdot R^{(3)}(t_3,t_2,t_1). \quad (47)$$

The 3^{rd}-order response function $R^{(3)}(t_3,t_2,t_1)$ contains many terms (Section 2.5) and the double-sided Feynman diagrams are particularly useful as they illustrate the response function in a intuitive way. The possible 3^{rd}-order Feynman diagrams for a three-level system shown in Fig. 11 describe the transition processes which have been discussed in Section 3.

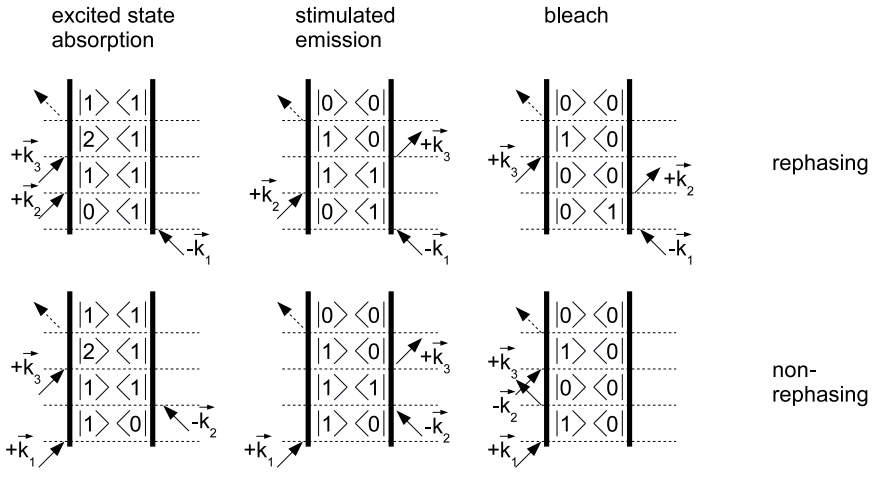

Figure 11: Feynman diagrams describing the possible transition processes of a three-level system.

In the most general case, three independent pulses are used with $\vec{k}$-vectors; $\vec{k}_1$, $\vec{k}_2$, $\vec{k}_3$. Then the signal fields $\vec{E}_{\text{sig}}$ are emitted in two different out-going directions:

$$\vec{k}_{s_{1/2}} = \pm\vec{k}_1 \mp \vec{k}_2 + \vec{k}_3. \tag{48}$$

The two different directions obey the rules for Feynman diagrams and describe phenomenological the same transition process but are distinguishable due to different $\vec{k}$-vectors as illustrated by the Feynman diagrams. The emitted signal with $\vec{k}_{s_1} = -\vec{k}_1 + \vec{k}_2 + \vec{k}_3$ is described by the so-called rephasing diagrams, top row in Fig. 11. The signal emitted in $\vec{k}_{s_2} = +\vec{k}_1 - \vec{k}_2 + \vec{k}_3$ direction is described by the so-called non-rephasing diagrams, bottom row in Fig. 11. If $k_1 \neq k_2 \neq k_3$, the outgoing signals are not collinear with any of the incident pulses unlike in the configuration for linear absorption. Thus usually an extra beam, a local oscillator (LO) is added to heterodyne the emitted signal, Fig. 12(a).

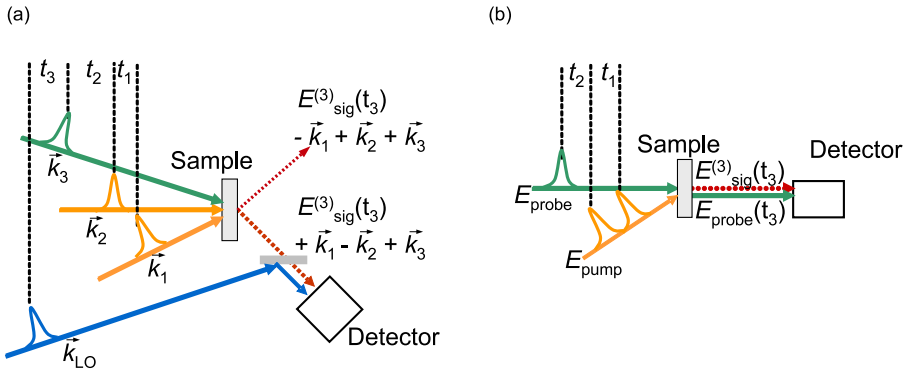

Figure 12: (a) Most general case of 3^{rd}-order nonlinear spectroscopy using three independent laser pulses to interact with the sample. The signals emitted are recorded in the two different directions which are not collinear with any of the incident beams. Thus, a fourth laser beam is used for heterodyned detection. (b) 3^{rd}-order nonlinear spectroscopy with pump-probe geometry. The emitted signals are all collinear to and heterodyned by the probe beam.

In a 3^{rd}-order nonlinear pump-probe spectroscopy experiment only two beams are directed onto the sample such that the first two interaction with the molecular system are caused by a single laser pulse or two collinear laser pulses, Fig. 12(b). Either way, the $\vec{k}$-vectors of the first two electric field interactions are equal, $\vec{k}_1 = \vec{k}_2 = \vec{k}$, such that the signals obeying the phase matching condition

$$\vec{k}_s = \mp\vec{k}_1 \pm \vec{k}_2 + \vec{k}_3 \tag{49}$$

$$= \mp\vec{k} \pm \vec{k} + \vec{k}_3 = \vec{k}_3 \tag{50}$$

are emitted in the same direction $\vec{k}_3$, which is furthermore collinear with the incident pulse responsible for the third interaction. Therefore, like in the configuration for linear spectroscopy, the generated 3^{rd}-order polarization is heterodyned by the electric field $\vec{E}_{\text{probe}}$.

5 2D IR spectroscopy methods

2D IR spectroscopy experiments have only been developed over the last two decades, although its useful application was already mentioned in 1976. [2] The first 2D IR spectra has then been measured in 1998 by Hamm, Lim and Hochstrasser [1,29] which was the beginning of the 2D IR spectroscopy research. All 2D IR spectroscopy methods require stable, ultrashort and intensive mid-IR pulses which is one of the main reasons why these techniques have not been developed earlier.
The first 2D IR experiment is based on a conventional pump-probe experiment with a narrow band pump pulse and will be referred to as the "Fabry-Perot" method (Section 5.1). Due to the simplicity of the Fabry-Perot method, it is still being used today. Over the last two decades a variety of 2D IR spectroscopy experiments and ideas have been developed. [1,7,8,17,28,30–32] Today, the most common alternative to the Fabry-Perot method is a Fourier transform method referred to as the "Photon-Echo" method which is based on a three-pulse photon echo experiment (Section 5.2). In general, both method yield the same information. [3,5] The purpose of the further developed 2D IR spectroscopy method here (Section 5.3) is to deliver a third method which on one hand results in 2D spectra with higher resolution than the Fabry-Perot method and on the other hand has an experimental handling that is easier than the one of the Photon-Echo method. All three methods will be briefly introduced and discussed within this section.

5.1 Frequency-frequency domain narrow band pump - broad band probe 2D IR spectroscopy method using Fabry-Perot filter

The 2D IR spectroscopy approach of Hamm, Lim and Hochstrasser is basically a narrow band pump - broad band probe experiment, schematically shown in Fig. 13. An ultrashort (typical pulse length of 100 fs) mid-IR beam is split into an intense pump beam and a weak probe beam. The narrow band pump pulse is created by a Fabry-Perot style etalon which allows sweeping the center frequency of the pump pulse across the pump frequency range of interest. The narrow band pump beam passes a delay line to define the time t_{pp} between the pump and the probe pulse. The broad band probe pulse bandwidth covers the whole spectral range of interest and overlaps spatially with the pump pulse on the sample generating the signal. The emitted signal will first be frequency dispersed in a spectrometer before being detected. By reasons of phase matching conditions in pump-probe geometry, the probe pulse is also the local oscillator (LO) for the heterodyne detection as always in (transient) absorption measurements. [5]

The data collection and processing is straightforward in this narrow band pump - broad band probe method which is one of the main advantages. The detector measures the signal at the probe frequency defined by the spectrometer such that the probe frequency axis is directly given. The pump frequency axis is given by the central frequency of the pump pulse that is controlled and scanned over the frequency range of interest by the Fabry-Perot filter. A light chopper at half the laser repetition rate is used to alternatingly

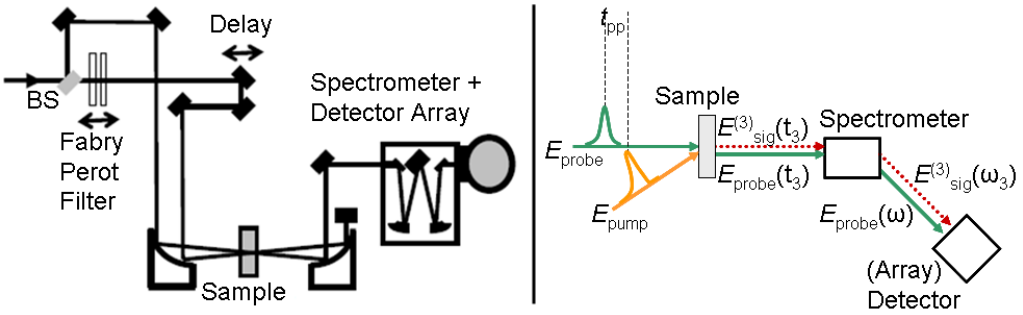

Figure 13: Narrow band pump - broad band probe 2D IR spectroscopy setup using a Fabry-Perot filter.

block the pump pulse such that the 2D IR spectra (difference spectra of probe absorption) are obtained. This method is referred to as a frequency-frequency domain method since the pump and probe frequency axis are directly given in the frequency domain and do not require additional data treatment.

5.2 Non-collinear time-frequency domain 2D IR photon-echo spectroscopy method

The main alternative to the Fabry-Perot method is the Photon-Echo method which describes a time-frequency domain method since only the emitted signal passing a spectrometer before detection is directly given in the frequency domain. The setup is schematically shown in Fig. 15. The Photon-Echo spectroscopy technique uses one independent pulse for each of the three interactions with the sample needed in 3^{rd}-order nonlinear spectroscopy. Two beam splitters (BS) are used in the ultrashort mid-IR beam to split the beam up into these three intense IR pulses. The time delay between the single pulses can be changed by means of two delay stages defining the delay time t_1 (coherence time) between the first two pump pulses and the time t_2 (population time) between the last pump pulse and the probe pulse which is equivalent to time t_{pp} in the Fabry-Perot method, Fig.14.

All three pulses spatially overlap and are focused on the sample. Obeying the phase matching conditions

$$\vec{k}_s = \mp\vec{k}_1 \pm \vec{k}_2 + \vec{k}_3, \tag{51}$$

the signal is emitted in two different directions describing the non-rephasing ($\vec{k}_s = +\vec{k}_1 - \vec{k}_2 + \vec{k}_3$) and rephasing ($\vec{k}_s = -\vec{k}_1 + \vec{k}_2 + \vec{k}_3$) processes.
A fraction of the incoming mid-IR beam is used as the local oscillator to interfere with the signal for heterodyned detection after passing the spectrometer. Different photo-echo geometries exist but the most widely used geometry is the so-called box-CARS geometry. [33]
Further data processing is needed since only the probe frequency axis is directly given by the spectrometer. The pump frequency axis has to be determined from the Fourier transformation of the data along the coherence time t_1 between the first two pump pulses.

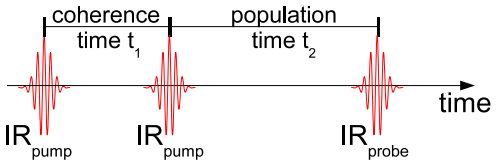

Figure 14: Pulse sequence for 2D IR spectroscopy measurements. The time delay between the two IR_{pump} pulses (the first two interactions) is defined as the coherence time delay t_1. The time delay between the second IR_{pump} pulse and the IR_{probe} pulse (time between second and third interaction) is defined as the population time delay t_2.

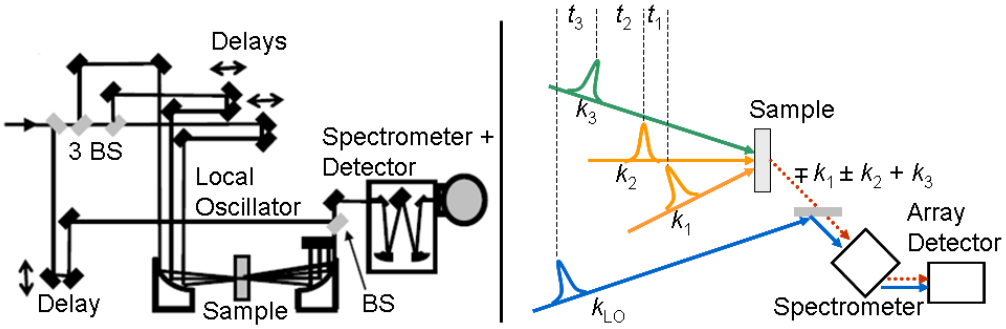

Figure 15: Non-collinear time-frequency domain 2D IR photon-echo spectroscopy setup

5.3 Collinear time-frequency domain 2D IR spectroscopy method using an interferometer

The Interferometer setup is based on a conventional pump-probe setup like the Fabry-Perot method. However, the Fabry-Perot filter is removed and exchanged by a modified Mach-Zehnder interferometer, see Fig. 16. The mid-IR beam is split into a probe and pump beam. The pump beam enters the interferometer and is divided to two parts and then spatially reunited at the output. These collinear pump pulses are temporally separated by a time delay t_1 (coherence time). Thus, three pulses will excite the sample but, in consequence of the collinear alignment of the two pump pulses, only two beam lines are focused onto the sample. As a result of the phase matching conditions, in the pump-probe geometry the emitted signal is heterodyned by the probe pulse. Therefore, the local oscillator for heterodyne detection is identical with the probe beam. The signal is measured directly in the frequency domain after passing the spectrometer. Similar to the Photon-Echo technique, the pump frequency axis needs to be determined by means of Fourier transform of the coherence time t_1 such that this method is also a time-frequency domain method.

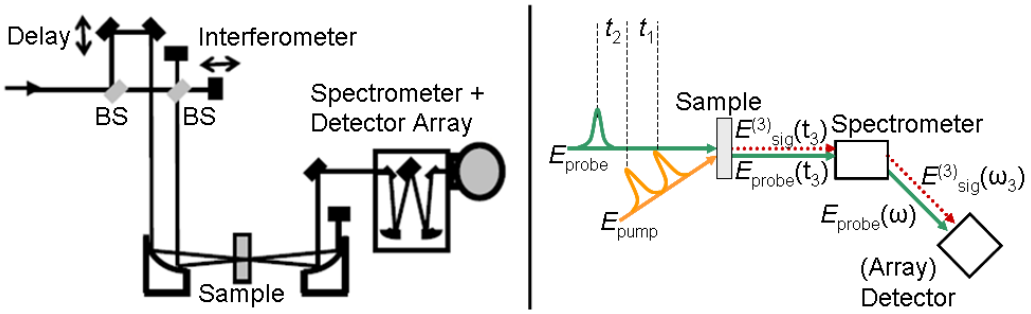

Figure 16: Collinear time-frequency domain 2D IR spectroscopy setup based on pump-probe geometry and using an interferometer

The underlying pump-probe setup in the Interferometer technique results in a simple setup and experimental handling. The interferometer splits the incoming pump pulse into two such that each interaction for the 2D IR signals is caused by a single pulse. In the pump-probe geometry the two pump pulses are collinear such that the non-rephasing and rephasing signal are emitted simultaneously in the same direction of the probe beam and the probe pulse heterodynes with the signal automatically before detection.

5.4 Discussion on the different 2D IR spectroscopy methods

The different setups clearly differ which affects the quality of the measured 2D IR spectra as well as the time to get the setup running, make the measurement and calculate the 2D IR spectra. The discussion here concentrates on three main concerns of the setups: the alignment, the correct phase for Fourier transform, and the time and spectral resolution of the measurements.
The different techniques have all been applied to dicarbonylacetylacetonato rhodium (RDC) molecules dissolved in hexane, Fig. 17(b). This molecule has been extensively studied by Tokmakoff and co-workers and suits well for this comparison. [17,30] The symmetric s' (2084 cm^{-1}) and asymmetric a' (2015 cm^{-1}) C≡O stretching vibrations are investigated for this purpose, Fig. 17(a). The sample has sufficiently narrow absorption bands, Fig. 17(a), such that all peaks in the 2D IR spectrum are spectrally resolved.

Alignment and setup geometry
3^{rd}-order nonlinear spectroscopy requires three interactions between the exciting pulses and the sample and additionally the emitted signal interferes with another beam/field for heterodyne detection. Thus, a maximum of four beams will be used in a 3^{rd}-order nonlinear spectroscopy. The simplest 3^{rd}-order nonlinear spectroscopy techniques are based on conventional pump-probe geometry with only two different beam lines. The complexity of the whole setup increases with each additional beam line. For both the Fabry-Perot and

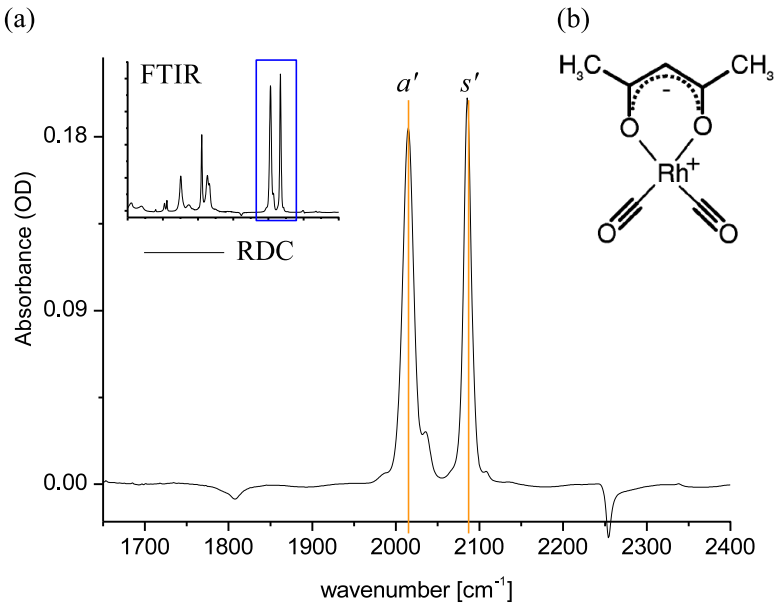

Figure 17: (a) The absorption spectrum of RDC shows the asymmetric (a') and symmetric (s') carbonyl stretching vibrations. (b) Chemical structure of dicarbonylacetylacetonato rhodium (RDC).

the Interferometer technique, which are based on a pump-probe geometry, only two beams have to be aligned. In contrast, the alignment of the Photon-Echo setup is much more challenging as it consists of four independent beams, one for each of the three interactions and one for the heterodyned detection. The effort of aligning four different beams, in return, results in the most versatile and sensitive experiment.
The setup geometry and the phase matching conditions define the direction of the emitting signal. In a photon-echo geometry where each interaction is caused by a single pulse, the phase matching conditions

$$\vec{k}_s = \pm\vec{k}_1 \mp \vec{k}_2 + \vec{k}_3, \tag{52}$$

are fulfilled such that the signal is emitted in $\vec{k}_{s_1} = +\vec{k}_1 - \vec{k}_2 + \vec{k}_3$ (non-rephasing process) and in $\vec{k}_{s_2} = -\vec{k}_1 + \vec{k}_2 + \vec{k}_3$ (rephasing process) direction. In pump-probe geometry, the first two interaction are caused by the same pulse (Fabry-Perot) or two collinear pulses (Interferometer), $\vec{k}_1 = \vec{k}_2 = \vec{k}$, such that the signal emits just in one direction, $\vec{k}_s = \pm\vec{k} \mp \vec{k} + \vec{k}_3 = \vec{k}_3$. Furthermore, the emitted signal in pump-probe geometry is the sum of the terms arising from rephasing and non-rephasing diagrams, while in the photon-echo geometry the emitted rephasing and non-rephasing signals can be measured separately.
Thus, the Photon-Echo method is more versatile than the pump-probe geometry methods. In practice, it has been shown that in order to obtain absorptive line shapes, which yield the highest spectral resolution, both contributions (non-rephasing and rephasing process) must be added. [30] Thus, in photon-echo geometry methods two signals have to be measured and

summed to obtain the 2D IR spectrum which is directly given in pump-probe geometry methods, Fig. 18.

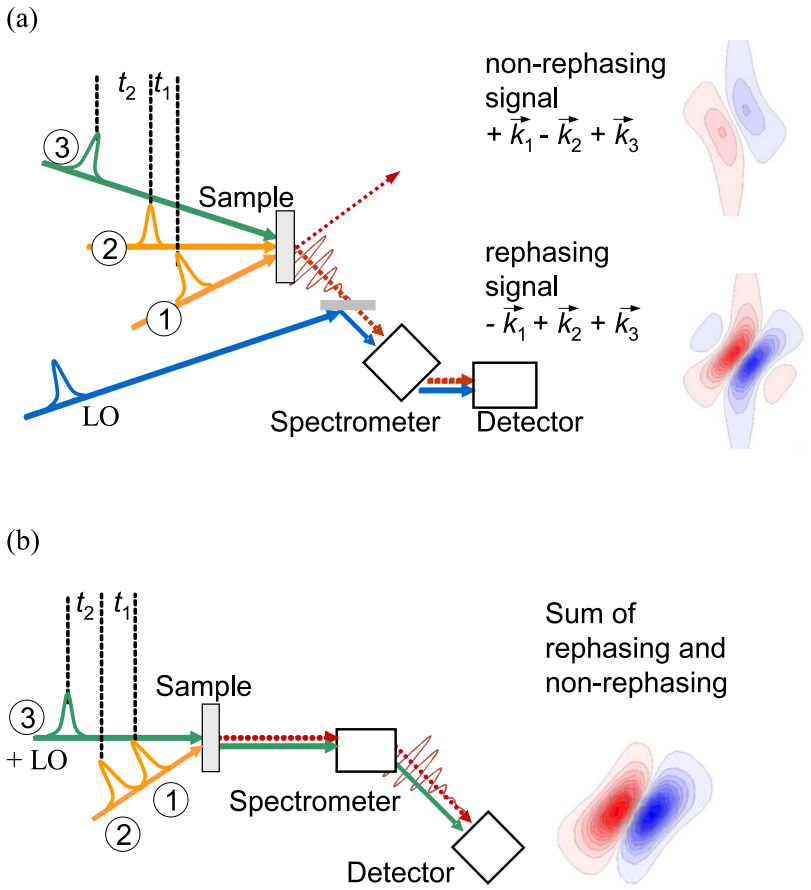

Figure 18: Schematic view of a 2D IR experiment with photon-echo geometry (a) and pump-probe geometry (b). In the photon-echo geometry, rephasing and non-rephasing signals are emitted in different directions. They can be recorded by the same detector after inverting the time order of pulses (1) and (2) and must be added to obtain purely absorptive 2D spectra. In the pump-probe geometry, pulses (1) and (2) are collinear, and the sum of rephasing and non-rephasing signals is measured directly. [34]

Another effect of the setup alignment concerns the heterodyned detection. The pulse(s) interacting with the sample should be intense. In photon-echo geometry, the intensity of each pulse can be controlled separately but most important for detection, the intensity of the LO pulse does not depend on the exciting pulses and can be treated totally independently. In pump-probe geometry, the LO is identical with the probe pulse and because of detector saturation the detector will limit the intensity of the probe pulse. This limitations makes 3^{rd}-order spectroscopy methods based on pump-probe geometry

less sensitive or in other words the Photon-Echo method is potentially the most sensitive 3^{rd}-order spectroscopy technique.

Relative phase between IR pulses
The 2D IR spectra are displayed in a frequency-frequency plot, however if the signals are measured as a function of time they need to be Fourier transformed to a function of frequency. Such a Fourier transformation requires exact knowledge about the phase of the signal which is transformed.
The pump frequency axis in the 2D IR spectrum is given directly by the pump frequency or the Fourier transform of the coherence time t_1 (time between first two interactions). The probe frequency axis is given by the Fourier transform of time t_3 (time between last interactions and emittance of the signal). It has been shown mathematically [27] that only the relative phase difference of the pulses responsible for the first two interaction and the relative phase difference of the pulse causing the third interaction and the local oscillator have an influence on the 2D IR spectrum.
The spectrometer used in front of the detector makes the Fourier transformation to obtain the probe frequency axis and therefore the relative phase between the "probe" pulse and the local oscillator has to be zero or known. In spectroscopy methods using a pump-probe geometry the "probe" pulse and local oscillator are identical such that there is no relative phase difference. In spectroscopy methods using the photon-echo geometry with independent "probe" pulse and local oscillator a relative phase difference can occur and has to be set to zero or known for corrections.
The pump frequency axis is directly given in the Fabry-Perot method and due to the pump-probe geometry there is no relative phase difference concerning the probe pulse and the local oscillator. Therefore, the Fabry-Perot method directly generates 2D IR spectra with correct phase and no need of further data processing.
Based on the pump-probe geometry, no relative phase difference between the probe pulse and local oscillator exist for the Interferometer method. However, to obtain the pump frequency axis one has to Fourier transform the measured data as a function of coherence time t_1 to a function of frequency ω_1 and therefore needs to know the relative phase difference of the pump pulses. Since the two pump pulses are collinear the relative phase difference is measured in a similar way as in FTIR spectroscopy and is easily obtained from an interferogram of the pump pulses that can be recorded alongside the experiment (Section 7.1.2).
The Photon-Echo method uses four different pulses such that the relative phase difference of the first two pulses and of the last two pulses needs to be known or set to zero. Besides the additional data processing, the determination of the relative phase difference requires considerable extra experimental effort. [33]

Time and spectral resolution
Fig. 19 shows the 2D IR spectra of the RDC molecule in hexane measured by the different techniques. All the spectra show the same peaks and therefore contain the same information. Nevertheless the resolution differs clearly between the frequency-frequency domain method and the time-frequency domain methods.

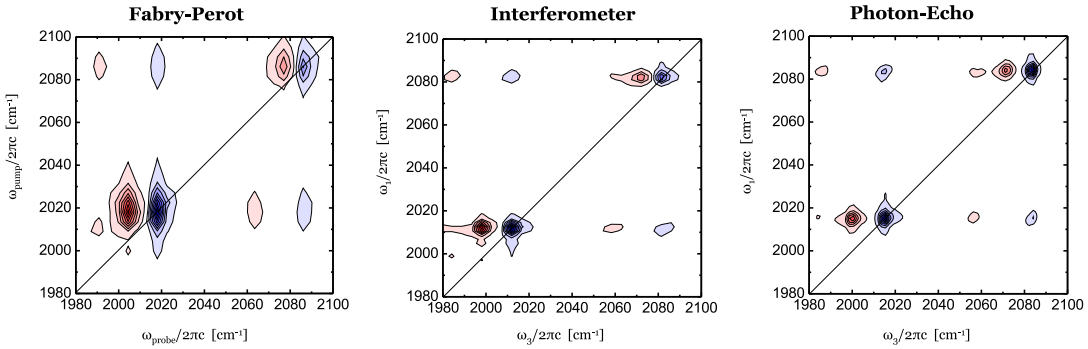

Figure 19: The 2D IR spectra of RDC in hexane are measured with the three spectroscopy methods. The 2D IR spectrum is recorded with (a) the Fabry-Perot method, measured in the research group of P. Hamm [5]; (b) the modified Mach-Zehnder interferometer method; and (c) the Photon-Echo method, measured in the research group of A. Tokmakoff using the Photon-Echo setup. [17,30] The 2D IR spectra show an on-diagonal peak doublet for each vibration as well as the cross-peaks which illustrate the correlation between the vibrations. Each peak doublet has a positive (red) and negative (blue) part.

Along the probe axis the peaks have de facto the same width, which is explained by the fact that all methods use a spectrometer and a detector to measure the emitted signal directly in the (probe) frequency domain. Therefore the grating of the spectrometer defines the range and resolution of the probe frequency axis.
The peaks in the spectrum measured by the Fabry-Perot method are broad along the pump axis. In contrast to the other two methods, the pump frequency axis is directly given by the Fabry-Perot filter. The pump pulse has a Lorentzian shape with a width $\propto \frac{1}{\text{duration}}$ such that a 1 ps time resolution considers a spectral width $\propto 10\text{cm}^{-1}$. Both, the Interferometer and Photon-Echo method use the Fourier transform of the coherence time t_1 to determine the pump frequency axis. The temporal and spectral resolution of the spectra that can be obtained by the Interferometer method is identical with the resolution obtained using the Photon-Echo method and is given by the range of the t_1 scan. The difference between the latter two methods concerns the sensitivity which is irrelevant in the example given in Fig. 19 since the signal is strong but it may become an issue for very weak signals.

Conclusion
Each of the methods introduced within this section has its advantages which makes it the best choice for a certain experiment. However, one has to be aware of the disadvantages of the method one uses to perform an experiment.
At the expense of being the simplest setup, the Fabry-Perot technique has some restrictions. The main advantage of this technique is that both frequency axes are directly given

such that the 2D IR spectrum is straightforward to obtain. The Photon-Echo method describes the most complex setup which needs most effort, in contrast it is the most versatile and sensitive technique. The Interferometer method describes an alternative method to both of the well established methods.
Both, the Interferometer and Photon-Echo method use two pulses for the first two interaction and the determination of the pump frequency axis requires phase determination and Fourier transformation of the coherence time t_1. In return one obtains 2D IR spectra with highest resolution. In addition, the two narrow band pump pulses resolve fast dynamics (<1 ps) which is not possible using the Fabry-Perot since its single pump pulse duration is typically longer than 1 ps. Due to the collinear geometry of the Interferometer method its experimental handling is far simpler than for the Photon-Echo method, however the versatility and sensitivity is limited.
In the measurements presented in Fig. 19 all spectra show the same peaks and therefore the information content of the 2D IR spectra is essentially the same. Nevertheless, it is possible that different peaks are displayed as a single broad peak if the resolution of the spectrum is low. In high resolution experiments close peaks will still appear well separated and can be clearly distinguished. The sensitivity is relevant for experiments with weak signals such that those signals might not rise above noise.
In Tab. 1, a short summary of the above discussed advantages and disadvantage for each of the three 3^{rd}-order spectroscopy methods is given.

	Fabry-Perot		**Interferometer**		**Photon-Echo**
+	most simple setup	+	simple collinear setup with only two beams	-	very complex setup with four independent beams
-	reduced spectral resolution in ω_1 and limited time resolution ($\approx$ 1 ps)	+	maximal spectral and time resolution	+	maximal spectral and time resolution
+	both frequency axes of the 2D IR spectra are directly given	+	relative phase between pump pulses given by their interferogram	-	relative phase of two pulse pairs must be determined independently
+/-	measures sum of rephasing and non-rephasing signals	+/-	measures sum of rephasing and non-rephasing signals	+	independent measurement of rephasing and non-rephasing signals
-	intensity of probe beam limited by detector (less sensitive)	-	intensity of probe beam limited by detector (less sensitive)	+	independent choice of four beam intensities, very sensitive
-	only one polarization degree of freedom	+	three polarization degrees of freedom	+	three independent polarization degrees of freedom
+/-	no multi-mode coherences	-	higher order signals overlap	+	higher order signals do not overlap

Table 1: Summary of the advantages and disadvantages of the different 2D IR spectroscopy techniques.

6 Phenomenological description of transient 2D IR spectroscopy

The systems studied in 2D IR spectroscopy experiments are assumed to be in equilibrium. The extension to transient two-dimensional infrared (T2D IR) spectroscopy implies the excitation of the systems to nonequilibrium. [18] Hence, in T2D IR spectroscopy the system is excited by an ultraviolet (UV) or visible pump pulse. Then a general 2D IR spectroscopy method[8] is applied, taking a "2D IR snapshot", to study the system while relaxing from UV excitation or while being excited. Since the additional excitation corresponds to two field interactions, the T2D IR methods describe a 5^{th}-order nonlinear spectroscopy experiment with UV_{pump}, IR_{pump} and IR_{probe} pulses, Fig. 20. [35]
Phenomenologically, the process of T2D IR spectroscopy methods is described in Fig. 20. The UV_{pump} pulse excites a certain fraction of molecules in the electronic ground state to the excited electronic state, Fig. 20(a). The following 2D IR snapshot is applied on this nonequilibrium system and will act on both, the molecules still in the electronic ground state and in the excited electronic state, Fig. 20(b). Thus, in a 2D IR spectrum of such a nonequilibrium system two groups of peaks appear as illustrated in Fig. 21(a). The peaks corresponding to the electronic ground state (equivalent to a 2D IR spectrum of a system in equilibrium) appear around $\omega_{\text{eq.}}$ and the ones corresponding to the excited electronic state around $\omega_{\text{ex.}}$.

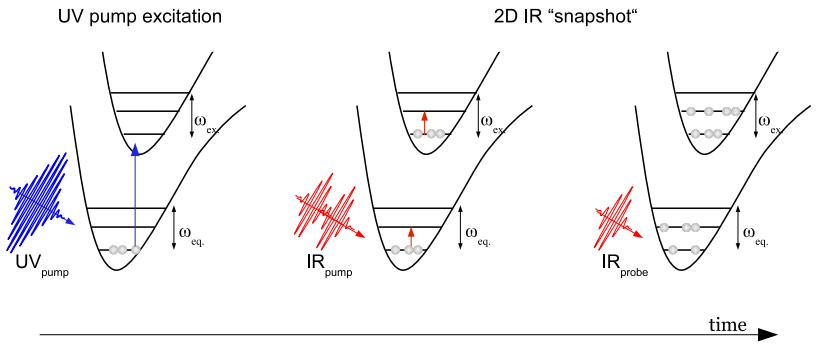

Figure 20: Illustration of the T2D IR spectroscopy measurement. First, a UV_{pump} pulse excites a certain part of the molecules of the electronic ground states to the excited electronic state. Then the 2D IR snapshot takes place as explained in Section 3 with the difference that the system is no longer in equilibrium such that the 2D IR snapshot acts on both electronic states. Therefore peaks belonging to the electronic ground state and peaks belonging to the excited electronic state appear in a T2D IR spectra, Fig. 21(c).

Analogous to a 2D IR spectrum, the T2D IR spectrum describe a difference spectrum of

[8] For example Fabry-Perot, Interferometer, or Photon-Echo method which have been discussed in Section 5.

two measurements where the 2D IR snapshot is taken once with preceding UV_{pump} pulse and once without UV excitation. Therefore, the 2D IR measurement is performed on a system in nonequilibrium and on a system in equilibrium. Fig. 21(c) illustrates the T2D IR difference spectrum of a single oscillator, for simplicity. A T2D IR measurement without preceding UV_{pump} pulse ($\hat{=}$ a general 2D IR measurement) on a single oscillator yields the spectrum shown in Fig. 21(b) which is denoted as the stationary 2D IR spectrum. The more interesting spectrum, Fig. 21(a), results when the UV_{pump} excites the system to nonequilibrium such that the IR frequency are shifted before the 2D IR snapshot is taken. [35]

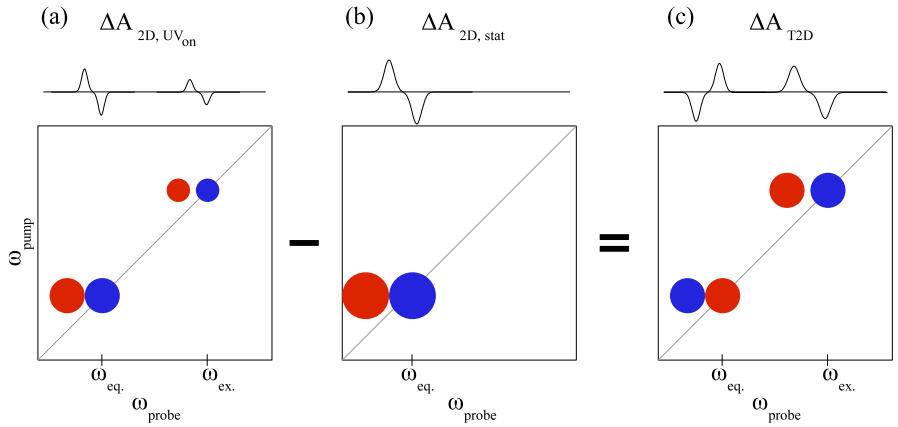

Figure 21: Schematical illustration of the generation of a T2D IR spectrum for a single oscillator. The 2D IR spectrum of the system in equilibrium ($\Delta A_{2D,\,stat}$) is subtracted from the 2D IR spectrum of the nonequilibrium system ($\Delta A_{2D,\,UV_{on}}$) due to the preceding UV_{pump} pulse. The sign of the peaks corresponding to the excitation in the ground state change upon the subtraction. The negative response is depicted in blue, and the positive response, in red.

In practice, a light chopper is used to block the UV beam alternatingly such that the 2D IR measurements with and without preceding UV_{pump} pulse are performed. Therefore two different data sets are recorded: $I_{UV_{on}IR_{sig}}$ and $I_{UV_{off}IR_{sig}}$. The $I_{UV_{on}IR_{sig}}$ data set describes the measurements where the 2D IR snapshot is taken on a nonequilibrium system, meaning that the UV_{pump} pulse excites the system first. The 2D IR snapshot performed on a equilibrium system with blocked preceding UV_{pump} pulse is described by the $I_{UV_{off}IR_{sig}}$ data set. The subscript IR_{sig} means that the 2D IR signal is given either by an additional IR light chopper as described in Section 3 or by a Fourier transformation (Section 7).
The absorption is described by Lambert-Beer's law and one typically normalizes the transmitted light I with a reference light, such that two additional data sets are recorded: $I_{UV_{on}IR_{ref}}$, and $I_{UV_{off}IR_{ref}}$. Eventually, one ends up with four data sets.
The stationary 2D IR spectrum, Fig. 21(b) is identical with a general 2D IR spectrum

since no preceding UV_{pump} pulse exists such that

$$\Delta A_{2D,\,stat} = -\log \frac{I_{UV_{off}IR_{sig}}}{I_{UV_{off}IR_{ref}}}. \tag{53}$$

The difference between the stationary 2D IR spectrum $\Delta A_{2D,\,stat}$ and the 2D IR spectrum with preceding UV_{pump} pulse $\Delta A_{2D,\,UV_{on}}$ yields the T2D IR difference spectrum: [18]

$$\Delta A_{T2D} = \Delta A_{2D,\,UV_{on}} - \Delta A_{2D,\,stat} \tag{54}$$

$$= -\log \frac{I_{UV_{on}IR_{sig}}}{I_{UV_{on}IR_{ref}}} - \left(-\log \frac{I_{UV_{off}IR_{sig}}}{I_{UV_{off}IR_{ref}}}\right) \tag{55}$$

$$\Delta A_{T2D} = -\log \frac{I_{UV_{on}IR_{sig}} \cdot I_{UV_{off}IR_{ref}}}{I_{UV_{on}IR_{ref}} \cdot I_{UV_{off}IR_{sig}}}\,. \tag{56}$$

In 2D IR spectroscopy experiments the pulse order is strictly given (the pump pulse(s) arrive before the probe pulse) and the IR_{pump}-IR_{probe} time delay changes within a measurement series to study the evolution in time. In T2D IR experiments, the pump-probe order is still given but two different pump processes exist: an UV pump and an IR pump process, such that the order of these pump processes can be changed. Therefore, the pulse order constitutes an additional parameter in a T2D IR spectroscopy experiment. Fig. 22 illustrates possible pulse sequences for T2D IR measurements based on a 2D IR Interferometer setup having two IR_{pump} pulses (Section 5.3). In (a) and (b), the UV_{pump} pulse arrives before the IR_{pump} pulses whereas in pulse sequence (c) the UV_{pump} pulse excites the system after the IR_{pump} pulses. The pulse order of the pulse sequence (a) and (b) are identical but symbolize two different ideas of possible measurements. In an experiment using pulse sequence (a), the UV_{pump}-IR_{pump} time delay varies and in an experiment with pulse sequence (b), the IR_{pump}-IR_{probe} time delay varies within the measurement series.

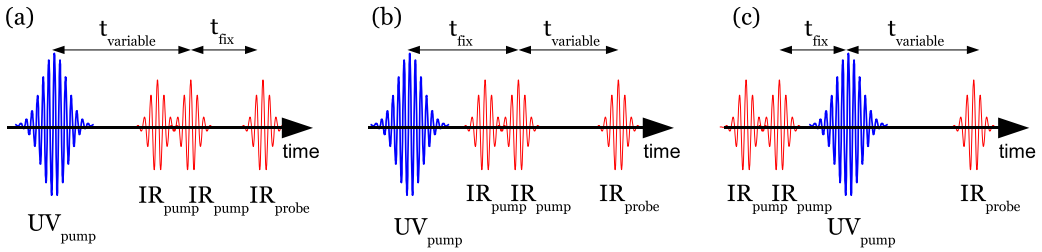

Figure 22: Illustration of the different pulse sequences used for T2D IR spectroscopy measurements. (a) and (b) describe the same pulse order but different experimental ideas. In (a) the UV_{pump}-IR_{pump} time delay will be varied and in (b) the IR_{pump}-IR_{probe} time delay will be varied throughout a measurement series. (c) describes a different pulse order where the IR_{pump} process takes place before the UV excitation of the system.

6.1 The UV_{pump}-IR_{pump}-IR_{probe} pulse sequence

The pulse sequences (a) and (b) in Fig. 22 are equivalent such that similar T2D IR spectra are obtained. The photo excitation upon the UV_{pump} pulse induces a frequency shift of the peaks along the diagonal as shown in Fig. 23.

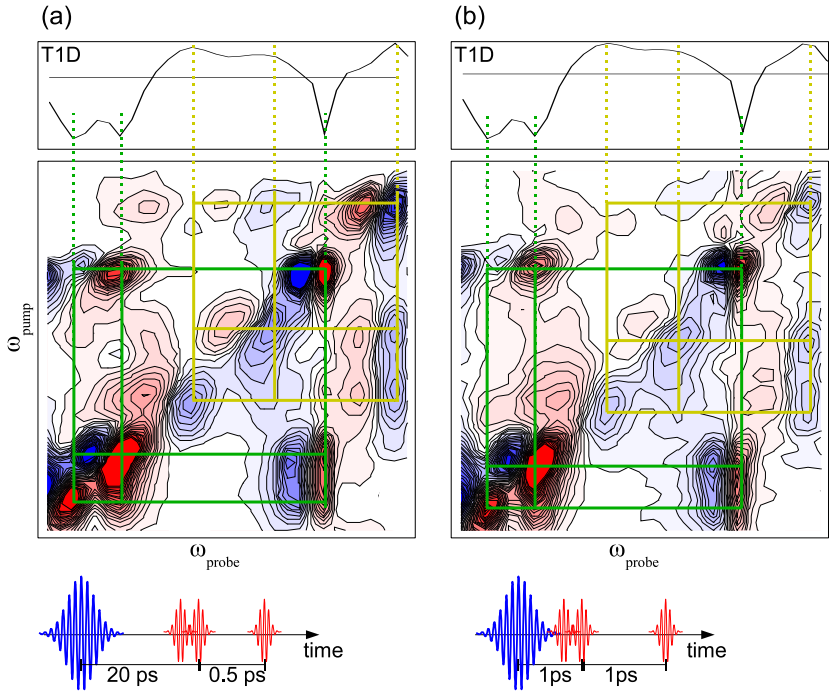

Figure 23: T2D IR spectra of a Re-complex dissolved in D_2O (see Section 8.1 for detailed information concerning the Re-complex). (a) Spectrum measured with UV_{pump}-IR_{pump} time delay = 20 ps and IR_{pump}-IR_{probe} time delay = 0.5 ps. (b) Spectrum measured with UV_{pump}-IR_{pump} time delay = 1 ps and IR_{pump}-IR_{probe} time delay = 1 ps.

In a typical T2D IR measurement, the time delay between the UV_{pump} pulse and subsequent 2D IR snapshot is long compared to the time delays within the 2D IR snapshot. Furthermore, the time delay between the UV_{pump} pulse and the 2D IR snapshot varies in a measurement series, Fig. 22(a). Therefore, photo reactions are probed by 2D IR snapshots instead of the absorption.
The time delay between the UV_{pump} and the 2D IR snapshot is short and does not vary within a measurement series regarding the pulse sequence illustrated in Fig. 22(b). The focus in such a measurement series lies on the shape change of a diagonal peak doublet while the population time t_2 in the 2D IR snapshot varies. [36,37]

6.2 The IR_{pump}-UV_{pump}-IR_{probe} pulse sequence

The inverting IR-UV-IR pulse sequence used for certain T2D IR spectroscopy experiments is quite useful as it can correlate the vibration bands of the reagent and the product in a photo reaction. The T2D IR spectrum in Fig. 24 presents such an experiment on a photo induced metal-to-ligand charge transfer of a carbonyl complex. The vibrational excitation induced by the IR_{pump} pulses takes place in the ground state. Therefore, the peaks are no longer shifted along the diagonal as before (Fig. 23) but experience a shift along the probe axis. This pulse sequence was first applied and presented by J. Bredenbeck et al. in 2003 [4] using the Fabry-Perot method (Section 5.1). The incident IR_{pump} pulses cause a population transfers from the vibration level $\nu = 0$ to $\nu = 1$ while the molecules are still in the electronic ground state. The subsequent UV_{pump} pulse causes an instantaneous frequency shift putting the molecules in the excited electronic state. Hence, the ground-state vibrations (reagent) and the excited state vibrations (product) are correlated by the pulse sequence.

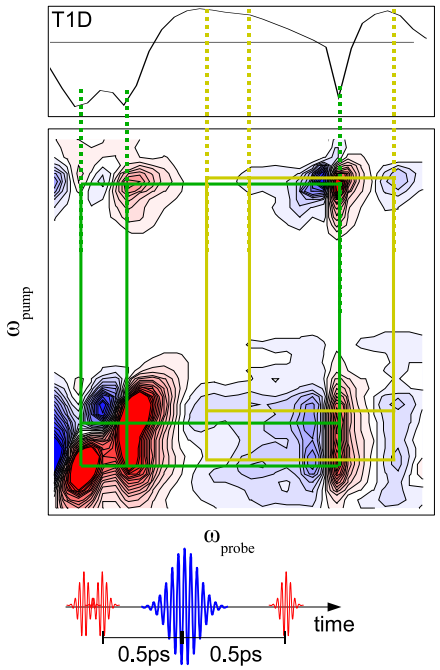

Figure 24: T2D IR spectroscopy measurement using IR-UV-IR pulse sequence performed on a Re-complex dissolved in D_2O. The spectrum is measured with a IR_{pump}-UV_{pump} time delay = 0.5 ps and a UV_{pump}-IR_{probe} time delay = 0.5 ps.

7 Setup for 2D and transient 2D IR spectroscopy measurements

Both 2D IR and T2D IR spectroscopy measurements require ultrashort (≈100 fs), tunable mid-IR pulses to pump and probe the sample. Additionally, T2D IR measurements need ultrashort (≈100 fs) UV pulses for the photo induced absorption processes. Both, the UV and IR pulses, are generated separately before entering the actual setup where the 2D/T2D IR measurement takes place. The main parts of the 2D/T2D IR spectroscopy setup are schematically illustrated in Fig. 25(b) and a picture of the different parts as they are arranged in the laboratory is shown in Fig. 25(a).

A commercially available Ti:Sapphire laser system (Spectra Spitfire) [38] generates ultrashort (100 fs) pulses at a wavelength around 800 nm with a single pulse energy of 750 μJ, and at a repetition rate of 1 kHz. These pulses are then divided by a beam splitter to a mid-infrared optical parametric amplifier (mid-IR OPA) setup and a "UV pulse generation setup" to generate the required mid-IR and UV pulses. Approximately one third of the pulse energy provided by the laser system is used for the mid-IR pulse generation.
The UV pulses have a wavelength of about 400 nm and are generated by second harmonic generation (SHG) in a BBO (β-barium borate) crystal. A mid-IR OPA creates the tunable femtosecond IR pulses. The mid-IR OPA is based on a white light seeded two-stage BBO-OPA where the signal and idler pulse are difference-frequency mixed in an $AgGaS_2$ crystal. This setup creates 80-100 fs short mid-IR pulses with 1-2.5 μJ energy. [25]

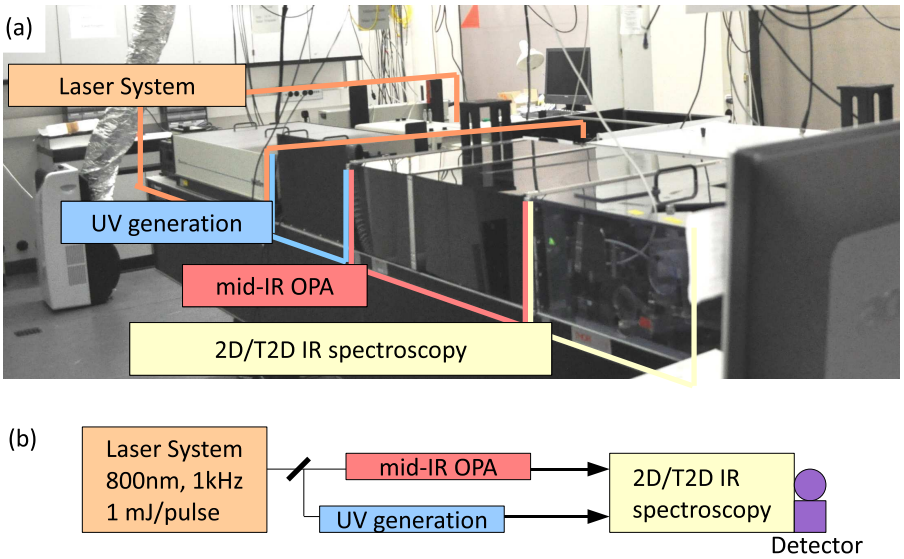

Figure 25: Overview of the single parts needed for 2D and T2D IR spectroscopy experiments. (a) picture of the different parts as they are set up in the laboratory and a schematic overview of the whole setup is given in (b).

7.1 2D/T2D IR spectroscopy setup

Fig. 26 shows a picture of the setup used for T2D and 2D IR spectroscopy measurements. Fig. 27 presents the schematic overview of the setup.
The IR beam (1) enters the 2D/T2D IR spectroscopy setup (orange line). A small fraction ($\approx 4\%$) of it is reflected at a wedged BaF_2 window (2) to obtain the broad band probe (dark red) and reference (green) beam. These two beams are vertically separated such that they pass the same pathways. The diameter of the probe and reference beam are enlarged by a factor of 1.5 in a telescope and both are tightly focused by parabolic mirrors onto different spots (vertically separated) on the sample.

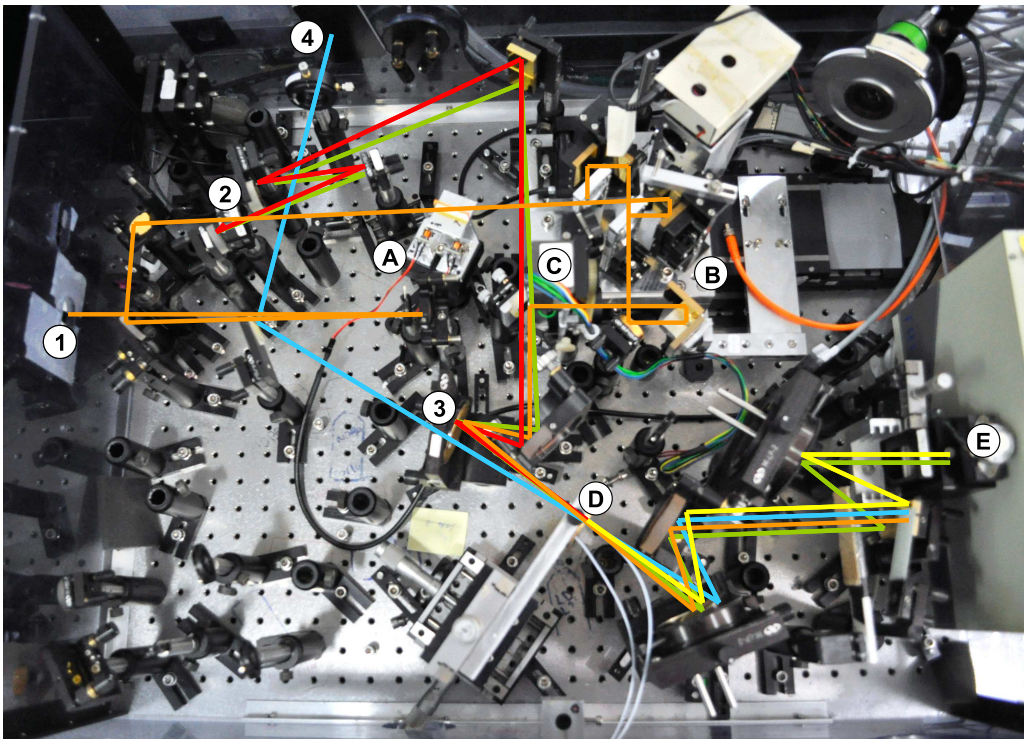

Figure 26: Picture of the 2D/T2D IR spectroscopy setup. (A) delay modulator, (B) modified Mach-Zehnder interferometer, (C) mount with half-wave plate, (D) sample in flow cell, (E) spectrometer and MCT detector. Orange line: IR_{pump} beam, dark red: IR_{probe} beam as fraction of pump beam, green: reference beam (IR_{ref}) as fraction of pump beam, blue: UV_{pump} beam, yellow: emitted signal beam.

The remainder of the IR beam (orange) is used as the pump beam and passes through a delay modulator (A, Section 7.1.1), to a modified Mach-Zehnder interferometer (B, Section 7.1.2). The interferometer separates the pump beam into two equal beams which leave the interferometer temporally separated due to the delay stage within the interferometer.

Then the pump beam passes another delay stage to define the time delays between the pump and probe beams. Depending on the performed measurement, the pump beam propagates through a zero order half-wave plate (C, Section 7.1.3), where the polarization of the pump beams can be changed with respect to the probe beam. Finally, The pump beam is focused in spatial overlap with the probe beam onto the sample in a flow cell (D, Section 7.1.4). The emitted signal beam (yellow) and the vertically separated reference beam (green) disperse in a spectrometer (E), and are detected by a mercury-cadmium-telluride (MCT) double-array detector with 2×32 pixels. [34]

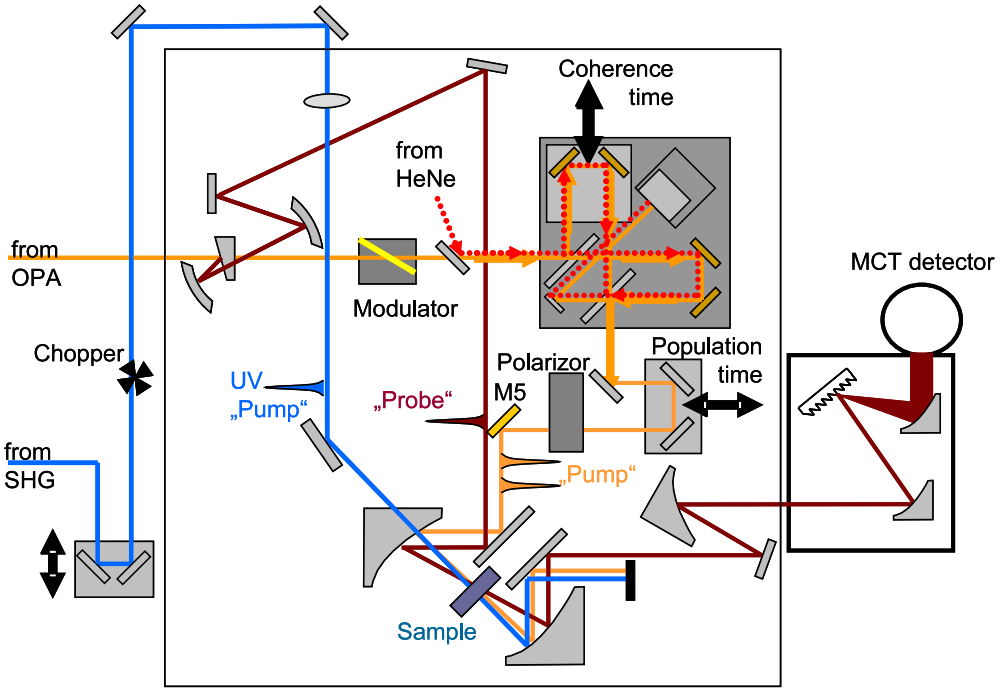

Figure 27: Schematic overview of the 2D/T2D IR spectroscopy part. Probe and reference beam are vertically separated and depicted as single dark red line. See text for description.

The temporally separated pump beams overlap spatially at the output of the interferometer such that the pump beams are collinear. Thus, only two beams (pump and probe) need to be overlapped in the sample and the used setup geometry is a pump-probe geometry. The IR_{probe} beam heterodynes and interferes with the emitted signal before the detection due to the phase matching condition.

In T2D IR spectroscopy experiments, an additional UV_{pump} beam is focused onto the sample in spatial overlap with the IR_{pump} and IR_{probe} beams. The UV beam is generated by SHG and passes a delay stage to define the temporal separation to the IR_{probe} beam. A light chopper is used to alternatingly block the UV beam to measure 2D IR spectra with and without preceding UV_{pump} pulse (Section 6).

7.1.1 Phase modulator device to suppress scattering and a light chopper in the UV beam

The main background in a 2D spectrum is scattering caused by a small amount of light from one or several pump pulses which interferes with the probe pulse on the detector. Thus, 2D IR spectroscopy setups with pump-probe geometry often use a light chopper to block every other laser shot of the static pump beam. [7] Then the difference between successive measurements is taken such that the signal remains and only scattering contributions due to the static pump beam remain. The scattering contributions of the static pump beam are removed by the t_1 Fourier transformation. The disadvantage of using a light chopper is that only half of the laser pulses are used to create a signal. An alternative strategy to circumvent these problems is to periodically invert the relative phase between the two collinear pump pulses and the probe pulse by π. [8] Then, adding the two signals results in cancellation of the scattering contributions.

Due to the broad band pump pulse a pure phase inversion (pure π-phase shift) over the whole range cannot be accomplished using time delay modulation. It has been shown in Ref. [34] that scattering suppression of more than two orders of magnitude over 10% bandwidth is still possible using a pseudo-phase inversion by changing the population time t_2 by half a period of the mid-IR carrier frequency ω_0. [39]

The pseudo-phase inversion is analytically described in Fig. 28. A signal is simulated in (a) without any scattering contributions and (b) shows the signal with scattering contributions. The signal is presented at the center frequency ω_0 with a spectral window of ± 10 % of ω_0. The scattered signals with a induced population time delay $t_2 = 0$ (blue) and $t_2 = -\frac{\pi}{\omega_0}$[9] (magenta) are plotted in Fig. 28(c). The pseudo-phase shift causes a destructive interference such that the sum of these two signals results in a signal with well suppressed scattering at the center frequency ω_0 and reduced scattering contributions on the edge of the spectral window (d). Fig. 28(e) shows the two scattered signals with $t_2 = 0$ (blue) and $t_2 = +\frac{\pi}{\omega_0}$ (green) and again the signals interfere destructively such that the sum yields a signal with suppressed scattering contributions. The two signals (d) and (f) describe a first order scattering suppression and are plotted together in (g). They almost perfectly overlap at the center frequency ω_0 however with increasing distance to ω_0 they interfere destructively such that their sum yields a signal with hardly any scattering at ω_0 and strongly reduced scattering within a range of $\pm$ 5 % of the center frequency, Fig. 28(h). Thus, the signal with second order suppression of the scattering contributions is the sum of signals recorded with $t_2 = 0$ (counted twice) and with $t_2 = \pm\frac{\pi}{\omega_0}$. [34]

In practice, a wobbling Zinc Selenide (ZnSe) window ("wobbler" [40]) is used in the pump beam in order to produce the t_2 delay changes, Fig. 27. It has been shown in Ref. [34] that the best cancellation for a single wobbler is obtained with second order suppression. Therefore, the signal has to be recorded with population time delay $t_2 = 0$ (twice) and $t_2 = \pm\frac{\pi}{\omega_0}$. These population times are achieved by the wobbler oscillating at one quarter

[9] The signal is shifted by half a period of the mid-IR carrier frequency ω_0.

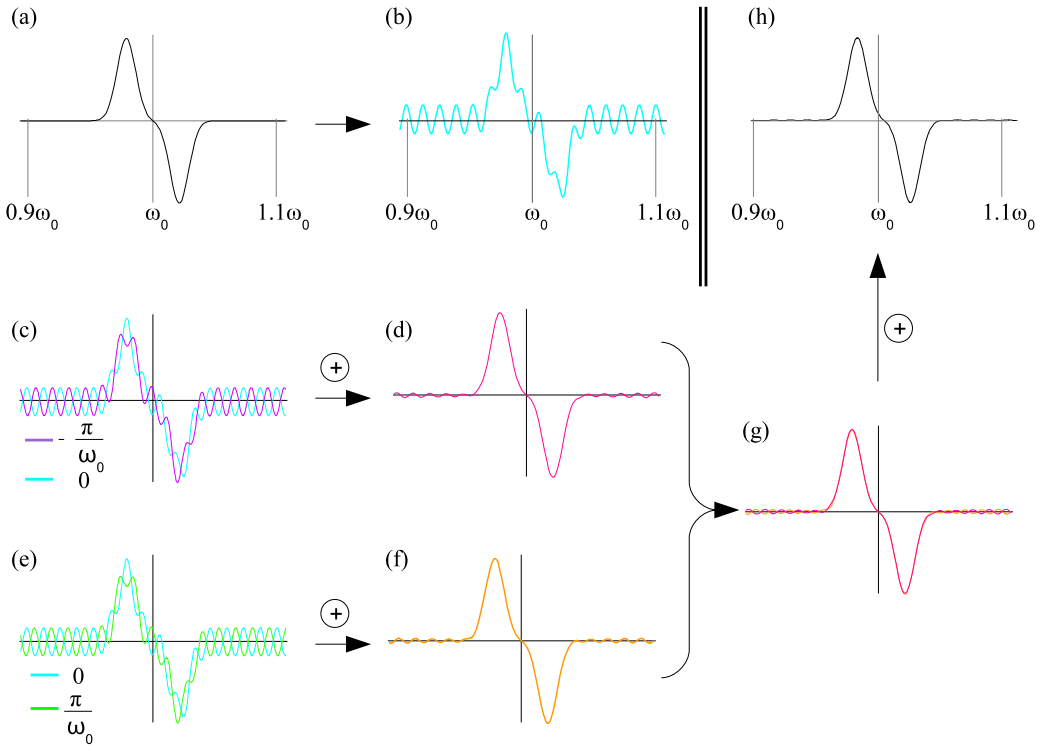

Figure 28: Analytical illustration of the pseudo-phase inversion on a simulated signal, see text for description.

of the laser repetition rate as illustrated in Fig. 29 such that four successive pump pulses experience the four wobbler states inducing the population time delays $t_2 = -\frac{\pi}{\omega_0}$, 0, $+\frac{\pi}{\omega_0}$, 0. Adding the signals of all four states with the same weight will yield the scattering suppressed signal shown in Fig. 28(h).

To summarize, the wobbler makes a shot-to-shot quasi-phase modulation and allows one to use all available pulses for the signal generation. The shot-to-shot modulation yields best correlation between the laser shots and hence the best possible signal-to-noise. The use of the above mentioned quasi-phase-cycle scheme therefore doubles the number of average in a given time interval and at the same time significantly suppresses the scattering contributions. [40]

In T2D IR experiments, the additional UV_{pump} pulse is periodically blocked by a light chopper such that a 2D measurement with and without preceding UV_{pump} pulse can be performed and then the difference is taken to obtain the T2D IR spectrum (Section 6). Due to the wobbler one has to make sure that every state is recorded at least once with and without preceding UV_{pump} pulse. Thus, the four wobbler states do not allow an alternating blocking of the UV_{pump} pulse or always the same wobbler states would experience the preceding UV_{pump} pulse. The obvious blocking scheme is to block four UV_{pump} pulses

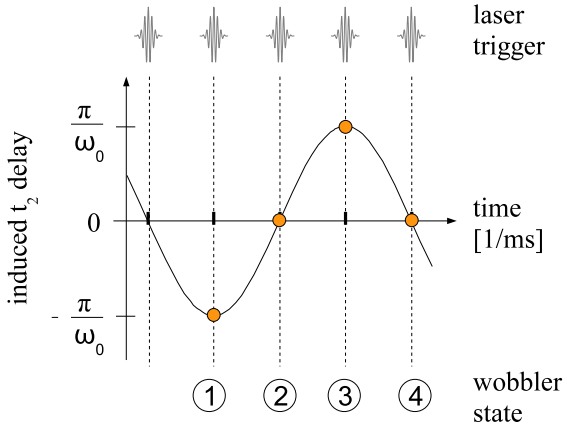

Figure 29: The wobbling delay modulator oscillates at on quarter of the laser repetition rate such that periodically the four states are generated which induce the population time delay order "$-\frac{\pi}{\omega_0}$, 0, $+\frac{\pi}{\omega_0}$, 0". The sum of the four recorded modulation state ("wobbler state") signals results in a second order suppression which gives the best cancellation using one wobbler in the setup. [34]

and let the next four through and so on, see Tab. 2(a). However, successive laser pulse intensities are most strongly correlated such that the quicker the switch between UV pumped and unpumped signals occurs the better the signal-to-noise. As mentioned before an alternating blocking scheme is not possible due to the four wobbler states. Thus, a blocking scheme where alternatingly three UV_{pump} pulses are blocked and the next three pass the light chopper is chosen which will lead to a periodic cycle for 12 pulses, Tab. 2(b). Due to this blocking scheme the frequency of the light chopper is synchronized to $\frac{1}{6}$ of the laser system repetition rate (1 kHz). To that end a frequency divider device was designed to obtain the correct frequency with respect to the laser repetition rate (Appendix A.1). With antisymmetric chopper blades one could think of other blocking schemes.

7.1.2 Interferometer

The modified Mach-Zehnder interferometer expresses the main advancement between the former Fabry-Perot and the actual setup. The pump frequency axis is defined differently which results in improvements of the temporal and spectral resolution of the measurements.

The interferometer has been designed as compact as possible and in such a way that the pulses in the two interferometer arms experience the same material dispersion: each of the beam is transmitted and reflected once at a beam splitter and experiences two gold mirror reflections. The IR beam is divided and then reunited by two equal calcium fluoride (CaF_2) beam splitters (BS) which show a 50% reflectivity over a wide infrared range, Fig. 30. Thus, the CaF_2 BS make the setup useful for a wide range of experiments with different

(a)													
wobbler state:	1	2	3	4	1	2	3	4	1	2	3	4	1
UV_{pump} pulse:	on	on	on	on	off	off	off	off	on	on	on	on	off
wobbler state with UV_{pump} pulse on:	1	2	3	4					1	2	3	4	

(b)													
wobbler state:	1	2	3	4	1	2	3	4	1	2	3	4	1
UV_{pump} pulse:	on	on	on	off	off	off	on	on	on	off	off	off	on
wobbler state with UV_{pump} pulse on:	1	2	3				3	4	1				1

Table 2: Table illustrates the combination of the four wobbler states and the UV_{pump} pulse. (a) Alternatingly four UV_{pump} pulses pass the light chopper and then four UV_{pump} pulses are blocked. The four wobbler states occur in order while the UV_{pump} pulse is present. (b) Antisymmetric order as the light chopper lets three UV_{pump} pulses pass and blocks the next three. After a cycle of 12 pulses the order repeats and each wobbler states occurs at least once with and without UV_{pump} pulse.

pump pulse wavelengths. Furthermore, the two generated pump pulses experience the same refraction and therefore will have identical energies.

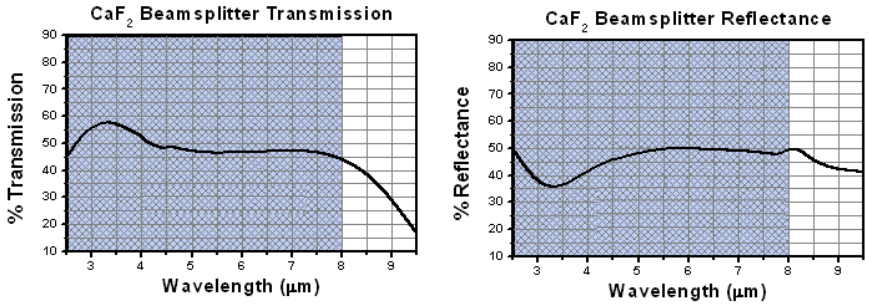

Figure 30: Reflectance (left) and transmission (right) curves for the 50:50 broad band plate beam splitters coated for $2-8\ \mu$m (Thorlabs Inc.), used in the modified Mach-Zehnder interferometer.

A schematic illustration of the interferometer is given in Fig. 31(a) and a picture of the setup in (b). The $\mathrm{IR_{pump}}$ beam (orange line) is divided into two pulses by the first BS (1). The reflected beam is directed to a delay stage (2) such that the time delay t_1 (coherence time) between the two pump beams can be varied. The second BS (3) reunites the two beams such that the pulses are collinear but temporally separated by the coherence time t_1. The interferometer setup has two outputs. One outgoing pump beam is focused onto the sample. The second output pump beam is directed to a pyroelectric detector (4). There, the two pump pulses produce an interference pattern which is related to the coherence time t_1 created by the delay stage. Furthermore, the phase needed for the Fourier transform of the 2D data can be automatically calculated from this interferogram.

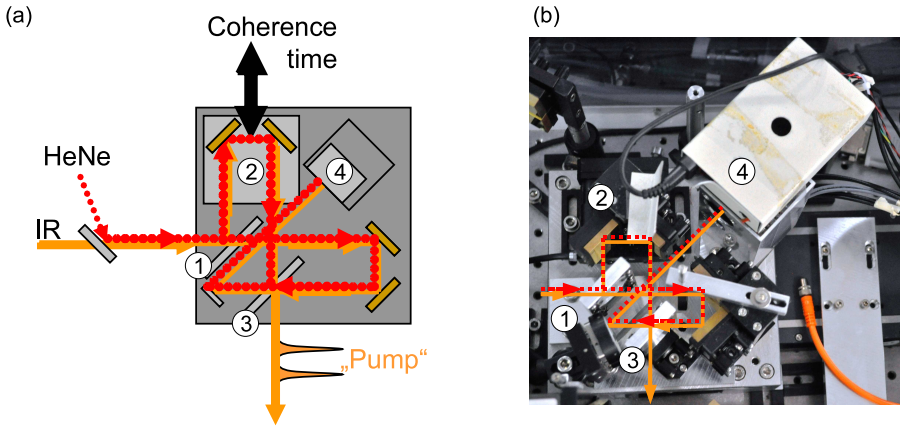

Figure 31: (a) Schematic illustration of the interferometer including the IR beam (orange line) and the HeNe (red dotted line). [34] (b) Picture of the interferometer setup. (1) First beam splitter, (2) gold mirrors mounted on a delay stage, (3) second beam splitter creating two output beams, (4) detectors.

The emitted signal has to be ordered and therefore an equidistant time grid related to the coherence time t_1 is needed. The delay stage is not sufficiently precise to ensure equidistant moving, especially not reproducible over several scans. Thus, a Helium-Neon (HeNe) continuous wave laser beam at 632 nm (red line in Fig. 31) is used to establish an equidistant time grid.

The HeNe beam enters the interferometer vertically separated from the pump beam such that it passes the same pathway and experiences the same time delay as the IR_{pump} beam. The HeNe beam generates an interferogram when reunited at the second BS. The fringes of the HeNe interferogram emerge every 2.11 fs such that these fringes create an equidistant time grid. The 2.11 fs range between two fringes is defined as a bin, Fig. 32(b). This techniques allows sorting the IR data according to the fringe number (bin) at the instant of pulse emission, meaning that the emitted signal can be assigned to a certain bin which is directly related to the coherence time t_1 between the two IR_{pump} pulses. In the end, all data within a given time bin is averaged. [34]

The interferometer can be scanned[10] relatively slowly or fast as it is used here. A Fast scan requires a fringe counting scheme that is not limited by the repetition rate of the laser system or the data acquisition card. Thus a stand-alone quadrature counting method based on Refs. [41,42] is used. A $\lambda/4$ wave plate producing circular polarization is inserted into the HeNe beam in the static arm of the interferometer, Fig. 32(a). The second BS combines the two HeNe beams and the sum of the circular and linear polarized HeNe beams is split into two perpendicular polarized components by a polarization cube oriented at 45° relative to the incident polarization, Fig. 32(a). The two signals have a relative phase difference of 90°, Fig. 32(b) and are used for continuous quadrature counting of the HeNe fringes at arbitrary speed and direction of delay changes. [34]

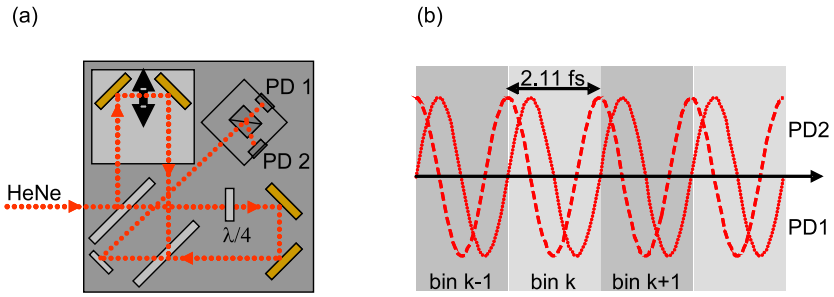

Figure 32: (a) Beam path of the HeNe beam propagating above the IR beam. Interference between a circular polarized beam ($\lambda/4$ plate in the static interferometer arm) and a linear polarized beam gives rise to the orthogonally polarized signals with a relative 90° phase shift (b) used for quadrature fringe counting. Two photo diodes (PD) are used to record orthogonally polarized HeNe signal. [34]

[10] Scanning the interferometer describes the moving of the delay stage through an interferogram. A relative slow scanning is, e.g., 2 fs delay in 5-10 ms. [34]

7.1.3 Motorized computer controlled mount for half-wave plates

The measurements presented in Section 8.4, use a zero order half-wave plate in the IR_{pump} beam line ((C) in Fig. 27) to change the polarization of the IR_{pump} beam with respect to the IR_{probe} beam. The zero order half-wave plate is fixed to a motorized computer controlled mount, Fig. 33, which can be preset to two different positions. Controlled by the computer the half-wave plate can be switched rapidly ($\approx 1/sec.$) between the two pre-defined positions which allows a quasi-simultaneous measurement of two sets of polarizations by changing the orientation of the plates. [43]

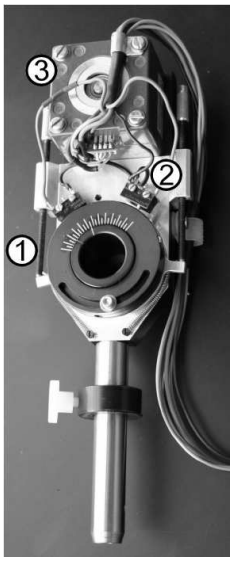

Figure 33: Motorized computer controlled mount for half-wave plates. (1) Fine thread for adjusting the preset polarizations, (2) position sensor, (3) stepping motor. [43]

7.1.4 Flow Cell

The pulse sequences in a T2D IR experiment require a high repetition rate of 1 kHz to enable sufficient averaging. Despite the high rate the sample has to be effectively exchanged between two consecutive pulse sequences to ensure that the sample has the same initial conditions. To fulfill these requirements J. Bredenbeck and P. Hamm designed a closed cycle flow cell system which can meet different demands based on its simple, reliable, and versatile construction principle. [44] In all the T2D IR spectroscopy methods this closed cycle flow cell was combined with a peristaltic pump (*ISM935C, Ismatex SA, Switzerland*). In some 2D IR spectroscopy measurements the continuous exchange of the sample is not necessary and the same flow cell is used in combination with a syringe to pull the sample solution into the flow cell, Fig. 34.

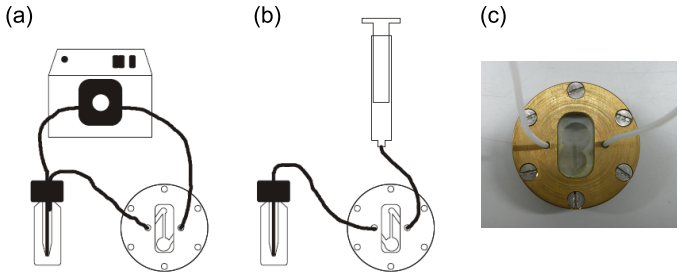

Figure 34: The flow cell in combination with a peristaltic pump (a) for T2D IR measurements and in combination with a syringe (b) for 2D IR or FTIR measurements. [43] (c) Picture of the flow cell.

7.2 Data acquisition and processing

The laser system runs at a repetition rate of 1 kHz such that every millisecond the fs pulses excite the sample and a signal is emitted. Based on the two array 32 pixel MCT detector the emitted signal and reference intensities are measured simultaneously and forwarded to the computer. All incoming data have to be ordered according to the actual parameters of the system (polarization state, wobbler state, coherence time, ...) which change between individual measurements.

Data acquisition
The basic idea behind the data acquisition is to create one "data matrix" for each of the possible parameter combinations, Fig. 35. The setup allows changing the polarization of the IR_{pump} beam between two settings (Section 7.1.3). The polarization states are denoted as parallel (par.) or perpendicular (perp.). The parallel polarization state describes the setting when the polarization of the IR_{pump} beam is parallel with respect to the polarization of the IR_{probe} beam. Analogous, the setting with the polarization of the IR_{pump} beam being perpendicular with respect to the polarization of the IR_{probe} beam describes the perpendicular polarization state. A T2D IR spectrum needs 2D IR measurements with and without preceding UV_{pump} pulse. Furthermore, one distinguishes four different phase delays (wobbler states) between IR_{pump} and IR_{probe} pulses and the simultaneous measured reference and signal intensities. The different polarization settings will lead to two different spectra such that 16 "data matrices" are needed just for one T2D IR spectrum corresponding to a pre-defined population time t_2 (time delay between IR_{pump} and IR_{probe} pulses), and UV_{pump}-IR_{probe} pulse time delay.

The "data matrices" have 32 columns and every column corresponds to one pixel of the array detector, Fig. 36. The lines represent the t_1 time bins which are defined by the HeNe grid and the interferogram (Section 7.1.2). Thus the columns are directly related to the probe frequency axis and the lines (bins) are indirectly related via Fourier transform to the pump frequency axis. Since t_1 is scanned quickly, the signal recorded at a given laser trigger usually fills one line in the corresponding "data matrix" and simultaneously

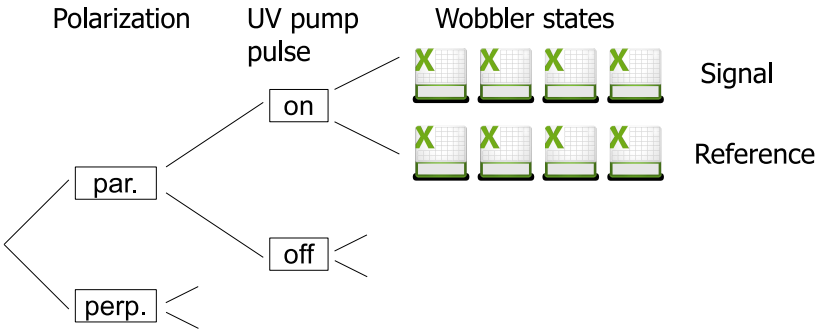

Figure 35: Diagram of possible parameter combinations leading to $2 \cdot 2 \cdot 2 \cdot 4 = 32$ "data matrices". The time delays UV_{pump}-IR_{pump} as well as t_2 (population time between the IR_{pump} and IR_{probe} pulses) are pre-defined for each spectrum. In a measurement series with different time delays each of the 2D/T2D IR spectra will at least require 16 "data matrices". The polarization states parallel (par.) and perpendicular (perp.) lead to different spectra. If sufficient either one polarization state can be measured.

the same line in the reference "data matrix" is recorded, Fig. 36(b). The number of bins is given by the t_1 range one scans. One bin is 2.11 fs wide such that for a t_1 range of 1 ps, 474 bins have to be recorded. The t_1 range has to be scanned until the emitted signal has been measured at least once for each bin (coherence time). If the emitted signal is measured several times for a certain bin then the average will be taken. In practice the t_1 range is typically scanned until every bin is averaged at least five times.

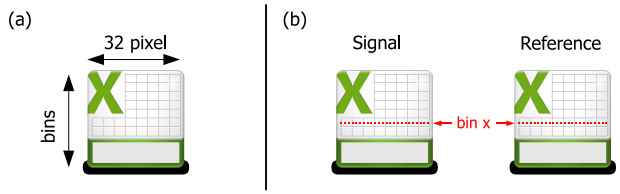

Figure 36: (a) Symbol of a bins×32 "data matrix" with each column corresponding to a pixel of the detector and the lines describing the bins of the defined HeNe grid, corresponding to the coherence time t_1 between the IR_{pump} pulses. (b) Based on the two array 32 pixel detector, every pixel will measure the intensity of the emitted signal at its probe frequency for a certain "bin x" and simultaneously the references signal is recorded.

Each parameter combination has four individual "data matrices", one for each wobbler state. These four "data matrices" are summed according to Section 7.1.1. Thus, out of the 16 "data matrices" recorded for a T2D IR spectrum one obtains the four independent "intensity matrices", Fig. 37,

$$I_{\mathrm{UV_{on}IR_{sig}}},\ I_{\mathrm{UV_{off}IR_{sig}}},\ I_{\mathrm{UV_{on}IR_{ref}}},\ I_{\mathrm{UV_{off}IR_{ref}}},$$

which are needed to compute the difference absorptive 2D or T2D data as discussed in Section 6 using Lambert Beer's law:

$$\Delta A_{2D} = -\log \frac{I_{\mathrm{UV_{off}IR_{sig}}}}{I_{\mathrm{UV_{off}IR_{ref}}}} \tag{57}$$

$$\Delta A_{T2D} = -\log \frac{I_{\mathrm{UV_{on}IR_{sig}}} \cdot I_{\mathrm{UV_{off}IR_{ref}}}}{I_{\mathrm{UV_{on}IR_{ref}}} \cdot I_{\mathrm{UV_{off}IR_{sig}}}}. \tag{58}$$

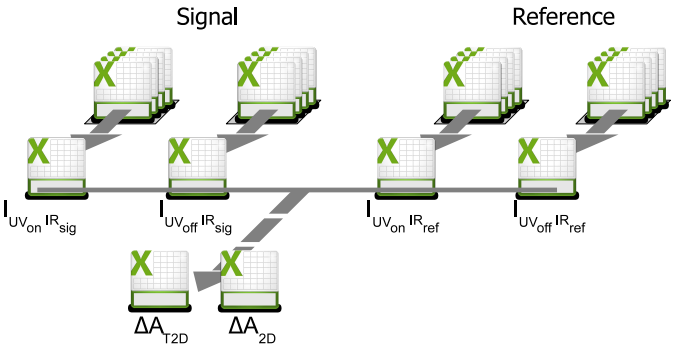

Figure 37: Diagram illustrating the process of the 16 recorded "data matrices" to obtain the desired difference absorptive data files ΔA_{T2D} and ΔA_{2D} for T2D IR and 2D IR spectra, respectively. The four matrices representing the different wobbler states are summed and yield the four individual "intensity matrices". These four matrices are needed to compute the difference absorptive data ΔA_{2D} and ΔA_{T2D} using Lambert Beer's law.

To obtain the desired 2D/T2D spectra some additional data processing is needed. So far, the y-axis (future pump frequency axis) of the 2D plot is still given as a function of the coherence time t_1, such that a 2D plot of a ΔA_{T2D} data is a time-frequency T2D spectrum as presented in Fig. 39(a). Therefore, the data as a function of coherence time t_1 has to be Fourier transformed to obtain the pump frequency ω_1 axis including possible phase corrections to obtain the correctly phased frequency-frequency T2D spectrum, Fig. 39(b). [34]

Data evaluation

As mentioned above, the ΔA_{2D} and ΔA_{T2D} data files are measured in time-frequency domain such that the data is given as a function of the coherence time t_1 and therefore a Fourier transformation has to be applied. The Fourier transformation requires the knowledge of the relative phase of the two collinear $\mathrm{IR_{pump}}$ pulses which is directly calculated from the pump pulse interferogram. [34] The calculations (Fourier transformation and data "tuning") to obtain the 2D/T2D spectra can be achieved with various mathematical software (e.g. Mathematica, Origin, MatLab). As subject of this Master thesis a program has been written which reads the ΔA_{2D} or ΔA_{T2D} data file and then directly shows the 2D or T2D IR spectrum even while the measuring process is going on. As an additional

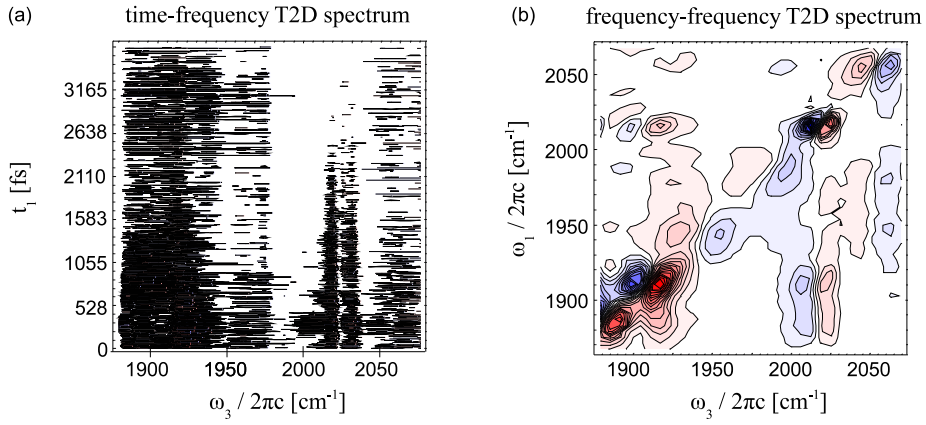

Figure 38: (a) A time-frequency 2D plot of a ΔA_{T2D} data file. (b) The wanted frequency-frequency 2D plot of the same ΔA_{T2D} data file after Fourier transformation of the coherence time t_1.

feature it allows to view vertical and horizontal cuts through the spectrum. Fig. 39 shows the working surface of this program.

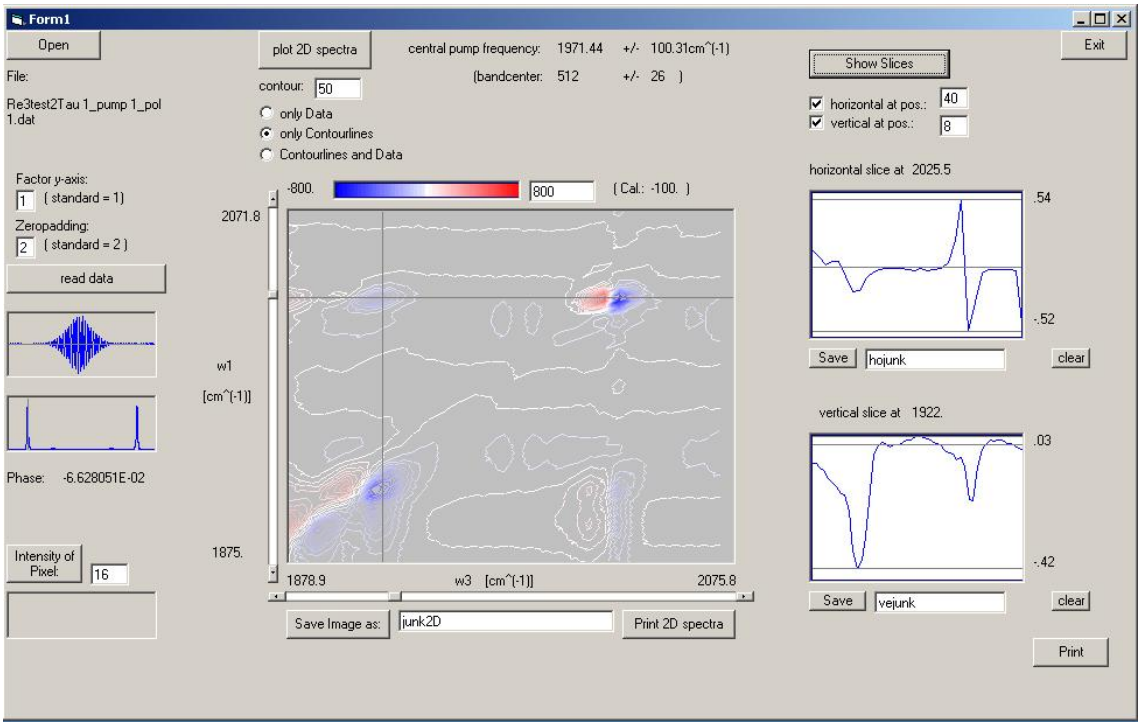

Figure 39: Working surface of the program to display the 2D or T2D spectrum. Additionally horizontal and vertical slices at a certain frequency can be plotted.

8 Measurements on [Re(CO)$_3$Br(bipy)]

Historically, the first T2D experiments have been done in the group of P. Hamm using the Fabry-Perot setup (Section 5.1). [1] Using the Interferometer setup introduced here, some of the measurements performed with the Fabry-Perot setup are repeated to compare results and test the setup. All measurements are performed on a Rhenium-complex (Section 8.1) dissolved in dimethylsulfoxide (DMSO). The results of the T2D IR measurements with preceding UV excitation are presented in Section 8.2, whereas in Section 8.3 a spectrum resulting from a T2D IR experiment with UV excitation after the IR$_{\text{pump}}$ pulses, is shown. Furthermore, it has been shown in previous experiments [23, 45] that the intensity of the peaks in a 2D or T2D IR spectrum depend on the polarization of the beams which is shown in Section 8.4 for the actual setup.

8.1 Rhenium-Complex

Rhenium (Re-) complexes have been well studied and used in many spectroscopic measurements due to its potential use in solar energy conversion. The photo induced metal-to-ligand charge transfer in [Re(CO)$_3$Br(bipy)] (bipy = 2,2'bipyridine) dissolved in DMSO (dimethylsulfoxide) is an interesting photoreaction to demonstrate T2D IR spectroscopy. [4] The molecular structure of the Re-complex is shown in Fig. 40(b).

The IR absorption spectrum of the [Re(CO)$_3$Br(bipy)] molecule in the ground state is shown in Fig. 40(a). The bands at 1890, 1910, and 2020 cm^{-1} have been assigned to $a'(2)$ (antisymmetric stretching of axial CO and equatorial COs), a'' (antisymmetric stretching of equatorial COs), and $a'(1)$ (symmetric stretching of all COs) modes, respectively. [21] The photo excitation at 400 nm promotes an electron of Re(l) to the bipyridine (metal-to-ligand charge transfer (MLCT)). The photo induced Re-complexes are excited to the singlet MLCT state (^{1}MLCT) which relaxes within 100 fs to the lowest lying triplet MLCT state (^{3}MLCT). [21] The quasi instantaneous change of the electronic structure, the cooling of the excess energy from ^{1}MLCT to ^{3}MLCT, and the subsequent slower shift due to solvation have been identified as the effects responsible for the change in vibrational frequency. [21–23] The vibrations in the excited ^{3}MLCT state are assigned with respect to vibrations in the electronic ground state. [23] Fig. 40(c) shows the UV pump - IR probe one-dimensional (T1D) spectrum of the Re-complex. The change of charge in the Re-complex leads to strengthening of the C=O bands and the photo induced frequency shift of the CO vibrations to higher frequencies is observed. The lifetimes of the excited ^{3}MLCT state of Re-complexes are much longer than 1 ns. [46]

8.2 T2D IR measurements with UV$_{\text{pump}}$-IR$_{\text{pump}}$-IR$_{\text{probe}}$ pulse sequence

Fig. 41(a) shows a 2D IR spectrum of the Re-complex. All peaks can be clearly assigned to the before defined CO vibrations a'', $a'(1)$, and $a'(2)$. Furthermore, the cross-peaks illus-

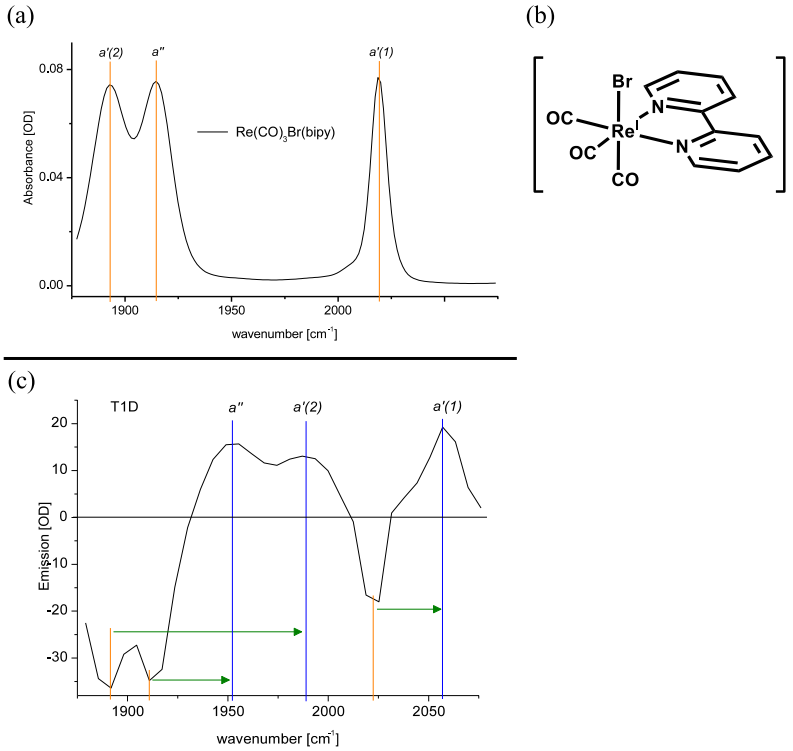

Figure 40: (a) FTIR absorption spectrum of the electronic ground state of [Re(CO)$_3$Br(bipy)]. The bands are labeled according to the text. (b) Illustration of the [Re(CO)$_3$Br(bipy)] molecule structure. (c) T1D spectrum, IR probe pulse occurs 20 ps after UV excitation. Green arrows depict the frequency shift due to the UV excitation.

trate the correlation between the bands. The spectrum in Fig. 41(b) presents the T2D IR measurement performed within the same frequency window. The photo induced frequency shifted peaks clearly appear on the diagonal as well as the cross-peaks which indicate the correlation of the bands in the excited electronic state. The peaks can be assigned to the peaks appearing in the one-dimensional UV$_{\text{pump}}$-IR$_{\text{probe}}$ (T1D) spectrum.

In Fig. 41 the frequency window was chosen to be large enough such that all C=O vibrations in the electronic ground and excited electronic state are shown. J. Bredenbeck et al. performed and published a T2D IR experiment on this Re-complex concentrating on the $a'(1)$ mode [47] which shifts from 2024 cm^{-1} in the electronic ground state to 2058 cm^{-1} in the completely solvated charge transfer state, Fig. 40(c). Since the former experiment was accomplished with a Fabry-Perot method, the results allow a direct comparison with the new established Interferometer method. The top row in Fig. 42 shows the T2D IR spectra resulting from the Fabry-Perot method and the T2D IR spectra measured with the new setup are presented below.

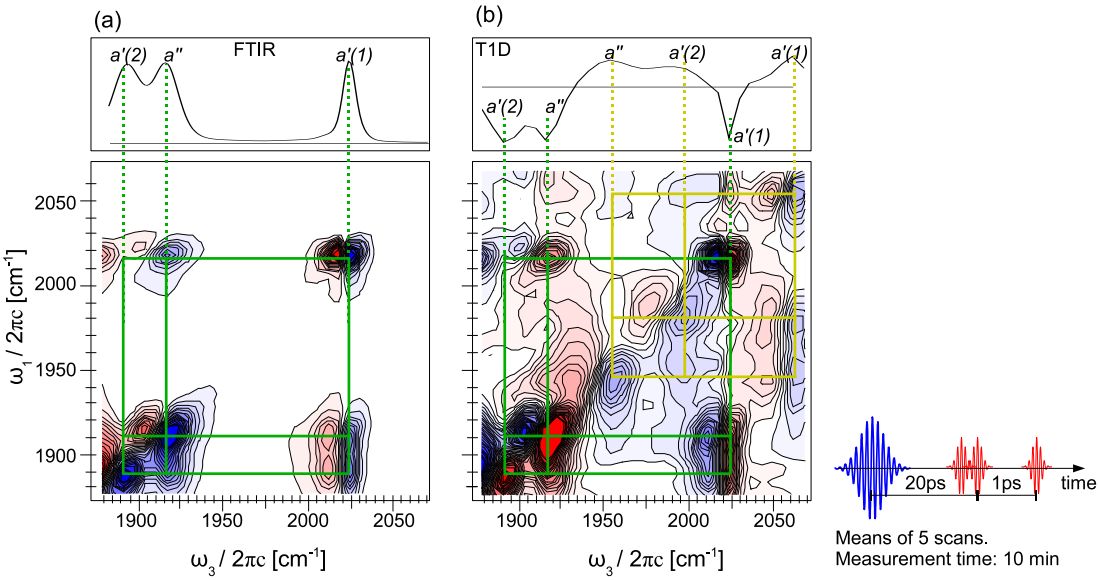

Figure 41: (a) 2D IR spectrum of the electronic ground state recorded with a IR_{pump}-IR_{probe} time delay of 1 ps. (b) T2D IR spectrum. A 2D snapshot is taken 20 ps after the UV excitation with a IR_{pump}-IR_{probe} time delay of 1 ps.

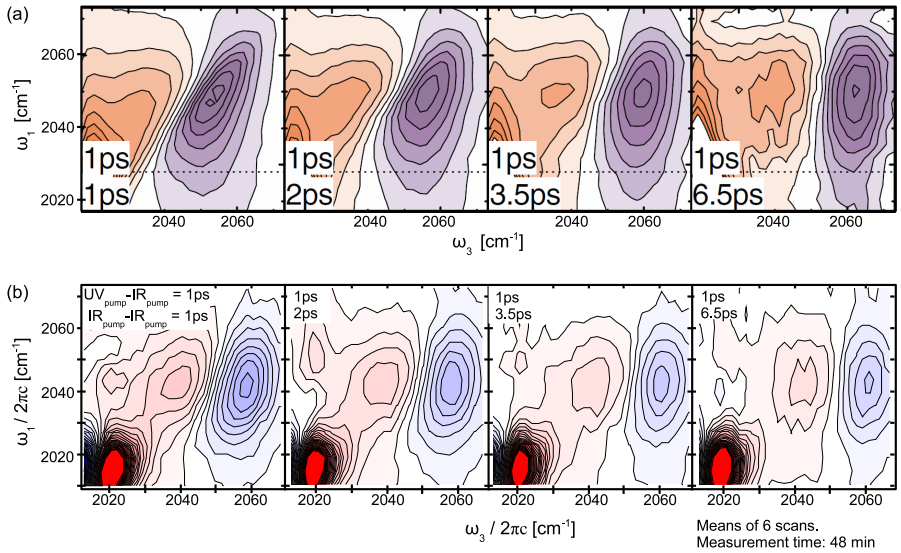

Figure 42: T2D IR spectra showing the measurement series with fix UV_{pump}-IR_{pump} time delay of 1 ps and varying IR_{pump}-IR_{probe} time delays from 1 ps up to 6.5 ps. The peaks present the highest frequency C=O vibration (symmetric stretch of all three CO's). Negative signals are depicted in blue, positive in red. (a) Spectra measured with Fabry-Perot method, taken from Ref. [47]. (b) T2D IR spectra measured using the Interferometer method.

The former experiment and its results are reproducible using the new setup. However the purpose of repeating the measurement series was to compare the resulting spectra. The new method is more sensitive, which results in more detailed peaks and the resolution is much higher, such that ground and excited state peaks are clearly separated in the new method, whereas they are not separated in the spectra measured by the Fabry-Perot method.

The excited state peaks in both sets of data are initially elongated along the pump frequency axis. In the Fabry-Perot method it is a result of the Fabry-Perot filter as discussed in Section 5.1. The resolution along pump frequency in the new setup is defined by the width of the mode in the excited state which narrows in time due to solvation and energy dissipation.

8.3 T2D IR spectroscopy with IR_{pump}-UV_{pump}-IR_{probe} pulse sequence

Experiments with inverted pump pulse order (IR_{pump}-UV_{pump}-IR_{probe}) have been performed to unambiguously assign shifted bands upon photo excitation to the corresponding bands in electronic ground state. With this experimental idea, it has been shown that the C=O vibration band order changes. [4]

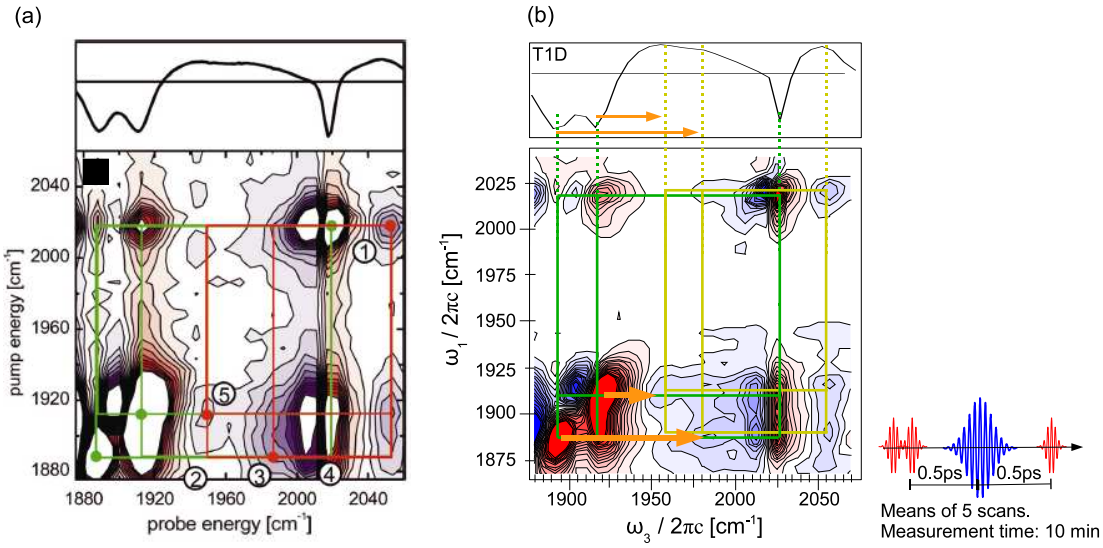

Figure 43: T2D IR spectrum with IR-UV-IR pulse sequence. (a) T2D IR spectrum measured with Fabry-Perot method and IR_{pump}-UV_{pump} = 2 ps and UV_{pump}-IR_{probe} = 2.5 ps. [4] (b) T2D IR spectrum recorded with IR_{pump}-UV_{pump} = 0.5 ps and UV_{pump}-IR_{probe} = 0.5 ps time delays using the Interferometer method.

As discussed in Section 6.2, the T2D IR spectrum presented in Fig. 43(b) illustrates that the peaks induced upon photo excitation after IR_{pump} sequence shift along the x-axis. The preceding IR_{pump} sequence selects vibrational bands in the ground state. The UV_{pump} pulse induces an electronic excitation which the vibrational bands withstand such that one observes the correlation of the vibrational bands of educt and product. [4] The spectrum measured with the Fabry-Perot method is presented in Fig. 43(a).

As in Section 8.2, the former experiment is reproducible and the surprising result that the band vibration order changes due to the UV excitation can be clearly observed (orange arrows in Fig.43(b)). The higher resolution of the new setup is remarkable. The new spectrum is unambiguous and leaves no doubt about the conclusions that have been made. The improvements of the current T2D IR spectra present the frequency shifted peaks in a clear manner as well as the cross-peaks.

8.4 Polarization dependence

The intensities of different peaks in 2D or T2D IR spectra are influenced by the polarizations of the different beams. [23, 45, 48] This polarization effects are interesting and useful for certain experiments. The 2D/T2D IR setup was designed such that it allows to change the polarization of the IR_{pump} beam with respect to the IR_{probe} beam.

Interactions between the electric fields of four laser pulses and up to three different transition dipole moments $\vec{\mu}$ take place in the T2D IR spectroscopy discussed here. Since both the dipole operator and the electric fields are vector quantities the signal depends on the relative orientation of light polarization and transition dipole moment at the times of interactions. The diagonal peaks originate if the IR_{pump} pulses and the IR_{probe} pulse interact with the same transition dipole moment $\vec{\mu}_i$. Cross-peaks originate from interactions of the IR_{pump} and IR_{probe} pulses with different transition dipole moments $\vec{\mu}_i$ and $\vec{\mu}_j$. [23] Therefore, if the T2D IR spectrum is recorded with perpendicular polarization of the IR_{pump} and IR_{probe} pulses the size of the diagonal peaks is reduced and the cross-peaks are more intense if the angle between the two transition dipole moments $\vec{\mu}_i$ and $\vec{\mu}_j$ is bigger than the magic angle ($= \arctan\sqrt{2} \approx 54.7°$). The angle between the transition dipole moments of the CO modes of the Re-complex discussed here is close to 90° due to their strong coupling. [23]

The two spectra shown in Fig. 44 as well as in Fig. 45 show the measurements with varied polarization settings to clarify the effect of the polarization. In Fig. 44 the UV-IR-IR pulse sequence and in Fig. 45 the IR-UV-IR pulse sequence have been used to perform the measurements.

The polarization of the IR_{pump} pulses is parallel in Fig. 44(a) and perpendicular in (b) with respect to the polarization of the IR_{probe} pulse. It is obvious to note that the diagonal peaks are enhanced in (a) and the cross-peaks are slightly weaker. In contrast, the spectrum in (b) shows weak diagonal peaks such that the photo induced peaks are hardly recognizable, but the cross-peaks are more intense.

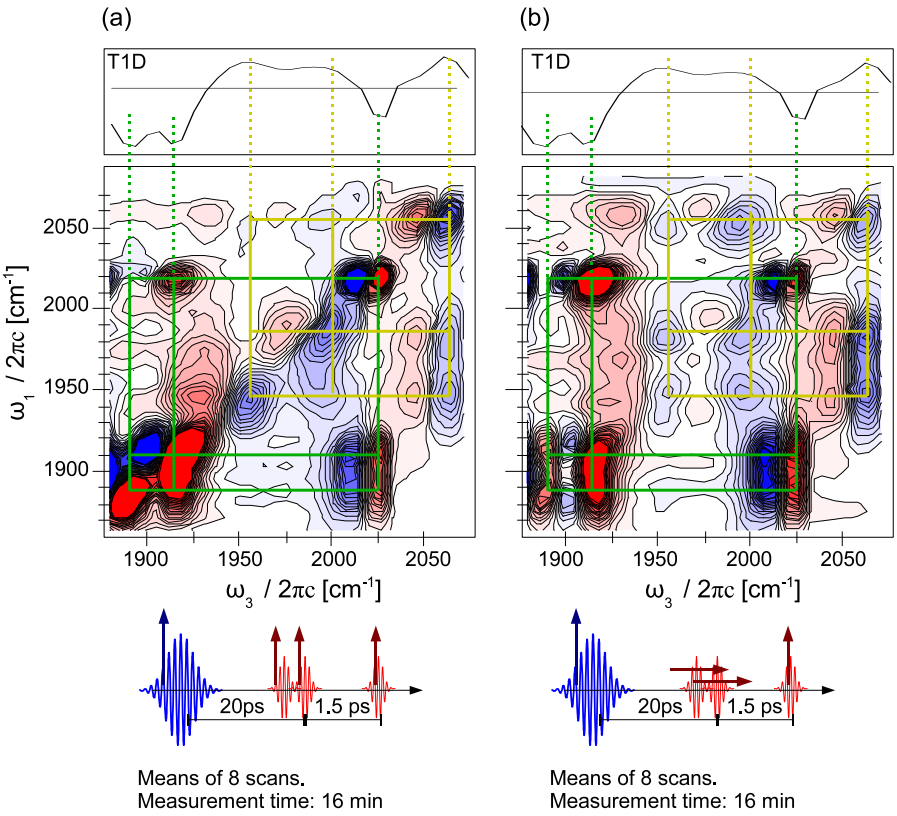

Figure 44: T2D IR spectra with UV excitation 20 ps before taking a 2D IR snapshot. The IR_{pump}-IR_{probe} time delay is 1.5 ps. (a) Parallel polarization. (b) Polarization of the IR_{pump} pulses is perpendicular with respect to the polarization of the IR_{probe} beam. This polarization setting enhances the intensities of the cross-peaks and weakens the intensity of the diagonal peaks.

The same observations are made for the inverted pulse sequence (IR-UV-IR) as illustrated in Fig. 45 where again in (a) the polarization of all pulses is parallel and in (b) the polarization between the IR probe and pump beams is perpendicular.

With respect to the changing band order upon photo excitation (Section 8.3) the two spectra with inverted pulse sequence and varying polarization setting are of interest. It has been shown in Ref. [23] and in Fig. 44 that the setting with IR_{pump} beam polarization being perpendicular with respect to the IR_{probe} beam polarization enhances the cross-peaks. Therefore, the peak (2) which clearly appears in Fig. 45(b) can be assigned to a cross-peak. Furthermore, peak (1) in Fig. 45(a) almost disappears in Fig. 45(b) which confirms the statement given in Section 8.3 concerning the band order upon photo excitation.

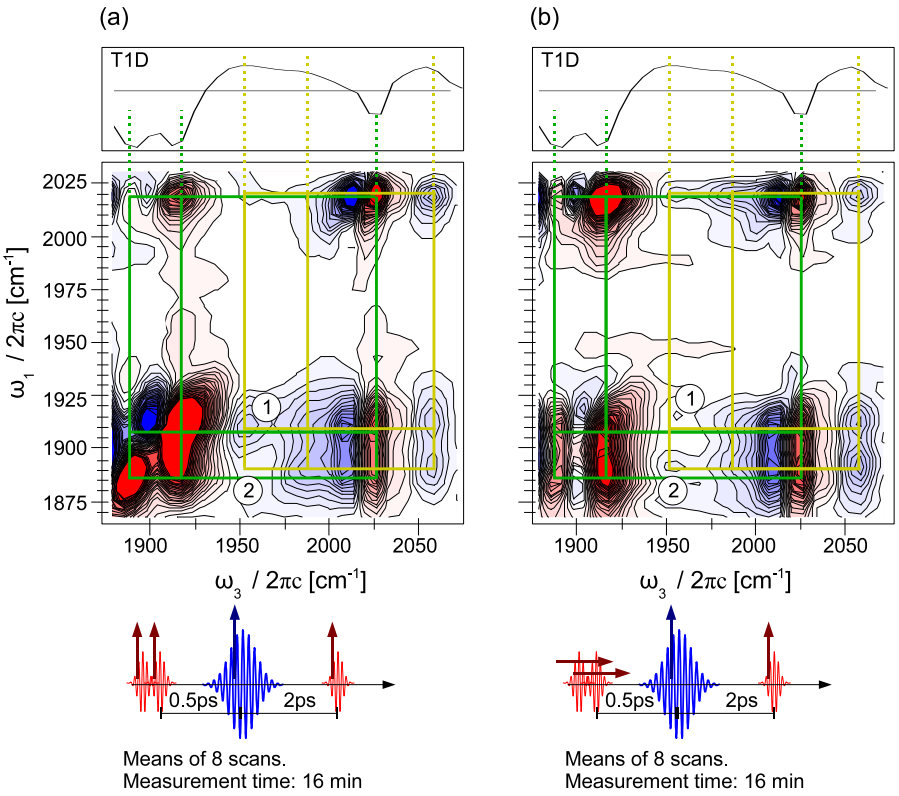

Figure 45: T2D IR spectra with inverted pulse sequence. The IR_{pump} pulses arrive 0.5 ps before the UV excitation and 2 ps after the IR_{probe} pulse follows. (a) Parallel polarization. (b) Polarization of the IR_{pump} pulses is perpendicular with respect to the polarization of the IR_{probe} beam. This polarization setting enhances the intensities of the cross-peaks and weakens the intensity of the diagonal peaks.

8.5 Conclusion on Measurements

All measurements presented confirm the functionality of the new setup as they reproduce previous results of Fabry-Perot method. The improvements show unambiguous peaks in the 2D or T2D IR spectra of the measurements. The higher sensitivity and resolution of the new setup has a remarkable influence as weak and close peaks appear clear and separated, respectively.

The resolution is the obvious point which can be compared between the different measurement techniques. As expected, no significant difference can be observed regarding the spectral resolution along the x-axis (probe frequency) in any 2D or T2D IR spectra. Both techniques use the same spectrometer and detector to record the probe frequency. The improvements along the y-axis (pump frequency) are significant using the interferometer generating two pump pulses. The spectral resolution depends on the coherence time t_1

which is covered by the two IR_{pump} pulses. The longer the covered coherence time delay t_1 the smaller the frequency steps $\Delta\omega$ along the pump frequency axis, given by the following relation

$$\Delta\omega = \frac{1}{2t_1}. \tag{59}$$

Thus, one tries to choose a long coherence time delay t_1, typically several ps. In 2D IR spectroscopy there is no restriction whatsoever longer t_1 delay will increase the measuring time. Furthermore, for a t_1 delay longer than a few ps the 3^{rd}-order polarization is typically zero and no further improvement concerning the spectral resolution can be observed. Due to the additional UV_{pump} pulse in T2D IR experiments the coherence time delay t_1 can no longer be chosen arbitrarily long. One of the two IR_{pump} pulses is at a fixed time delay $t_{\text{UV-IR}}$ with respect to the UV_{pump} pulse. The other IR_{pump} pulse moves and defines the coherence time delays t_1 between the two IR_{pump} pulses. In the case where $t_{\text{UV-IR}}$ is shorter than t_1 the pump pulse order changes such that one IR_{pump} pulse arrives before the UV_{pump} pulse and the second, the fix IR_{pump} pulse will still interacts with the sample after the UV excitation as illustrated in Fig. 46.

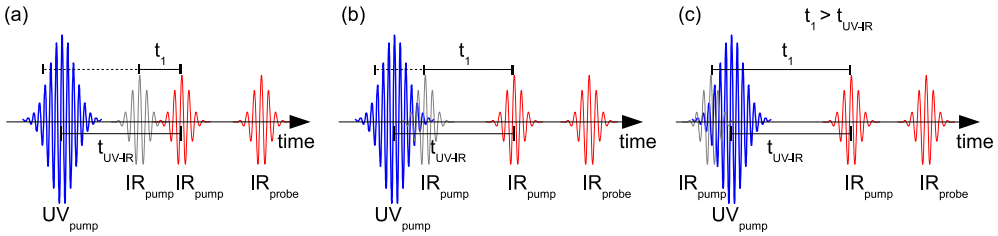

Figure 46: Illustration of the changing pulse order. The pulse order will change as soon as the time delay $t_{\text{UV-IR}}$ between the UV_{pump} and the fix IR_{pump} pulse is smaller then the coherence time delay t_1 between the two IR_{pump} pulses. The gray IR_{pump} pulse illustrates the moving of the IR_{pump} pulse as it changes position within (a)-(c). Changed pulse order in (c).

Thus, the maximal coherence time delay range of the IR_{pump} is limited by the time delay $t_{\text{UV-IR}}$ between the fix IR_{pump} and UV_{pump} pulse. However, this restriction does not affect T2D measurements with inverted pulse sequence (IR-UV-IR) since both IR_{pump} pulses excite the sample before the UV excitation, and it is only limited to T2D measurements where the time delay $t_{\text{UV-IR}}$ is short, typically below 2 ps.

The effect of this pulse order change within a measurement is not studied so far. Fig. 47(b) shows a measured signal as function of time where the covered coherence time delay t_1 is 3.5 ps and the time delay between the UV_{pump} and fix IR_{pump} pulse $t_{\text{UV-IR}}$ is only 1 ps, Fig. 47(a). The measured data shows no obvious effects at the instant of time (1 ps after the fix IR_{pump} pulse) where the UV_{pump} interacts with the sample, blue arrows in Fig. 47(b,d). To consider the signal without influence of the UV_{pump} pulse in between the two IR_{pump} pulses one can convolute the measured signal by a Gaussian function which takes the signal to zero at t_1 =1 ps, Fig. 47(d). The T2D spectrum with the data being

modified through the Gaussian function is shown in Fig. 47(e) and it results with much less spectral resolution. In contrast, Fig. 47(c) shows the T2D spectrum of the measured signal without any modification by a Gaussian convolution.

The T2D spectrum without forcing the signal to zero at t_1 times bigger than $t_{\text{UV-IR}}$ is much higher resolved and no influence of the changing pulse order could be clearly observed. Therefore no concluding statement can be given and the understanding of this effect will require some further study.

A further improvement concerns the measurement time. Usually, publications do not provide any information concerning the time it takes to measure a certain spectrum and how many times a resulting spectrum was averaged. Fortunately, the measurements performed using Fabry-Perot method and presented here have been accomplished in this study. From this experience it can be said that the time needed to record a comparable 2D/T2D IR spectrum is about three times less. Therefore, the Interferometer method saves a lot of measuring time or in the same time much better 2D/T2D IR spectra result due to higher averaging can be achieved.

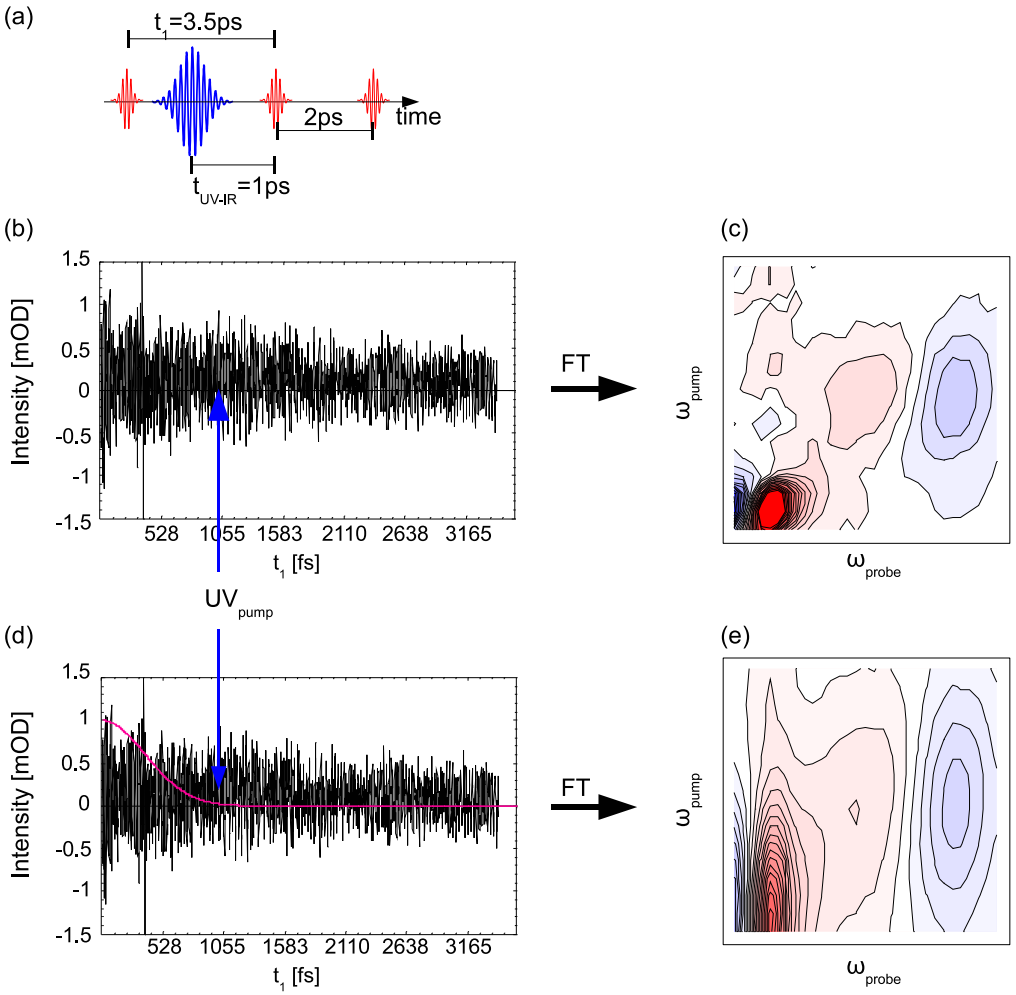

Figure 47: Illustration to observe the influence of changing pulse orders within a measurement. (a) Shows the time delay parameters and one notes that the IR_{pump} pulse happens to interact with the sample before the UV excitation takes place. The recorded signal is shown in (b) and (d) whereas in (d) a Gaussian function (red) is added to illustrate the convolution of the recorded data with the Gaussian function to take the data to zero at the instant of time where the UV_{pump} pulse interacts with the sample, blue arrows. No significant influence of the UV_{pump} pulse can be noticed in the recorded data (b) and (d). The T2D IR spectra are shown in (c) without modification of the data and in (e) as convolution with the Gaussian function. The loss of resolution in (e) is remarkable but the spectrum in (c) does not show any obvious effects of the changing pulse order within the measurement.

9 Conclusion and outlook

The T2D/2D IR spectroscopy method works very well and represents a reliable alternative to the established methods. The setup is already being used for actual 2D IR research within this research group [36,37] and will very likely find its way into other research groups as well since it provides the researcher quickly with reliable 2D spectra.
2D IR spectroscopy became a wide spread spectroscopy technique over the last decades and several different implementations of the setup exist. [1,3–8] Transient 2D IR spectroscopy is in the early stages of development and it is achieved only in few research groups. Based on a Fabry-Perot 2D IR setup transient 2D IR spectroscopy has been performed earlier. [4,18,23,24,35] The extension of the most versatile and sensitive Photo-Echo 2D IR setup to transient 2D IR has also been accomplished [49,50] but the experimental handling of this 2D IR spectroscopy method is already challenging. Therefore, the new transient 2D IR spectroscopy method introduced here describes for the first time a new possibility for T2D IR spectroscopy experiments with a spectral resolution that is unattainable by a T2D IR Fabry-Perot spectroscopy method and a rather simple experimental handling.

While performing the first measurements, a restriction concerning the time delay parameters of the T2D IR setup has been noted. The time delay $t_{\text{UV-fix IR}}$ between the UV_{pump} and the fixed IR_{pump} pulse has to be longer than the coherence time delay t_1 between the two IR_{pump} pulses. If not, the pulse order will change as illustrated in Fig. 48. The coherence time delay t_1 is related to the resolution such that if the t_1 scan range is chosen to be short it will result in less spectral resolution (Section 8.5). However, this effect occurs only for measurements with a UV-IR-IR pulse sequence and a short time delay $t_{\text{UV-fix IR}}$ between the UV_{pump} and fixed IR_{pump} pulses, typically below 2 ps.

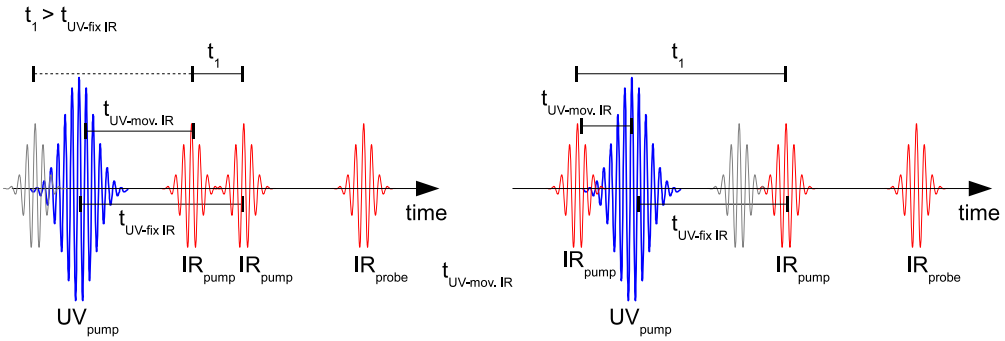

Figure 48: Illustration of changing pulse order with the coherence time delay t_1 being longer than the time delay $t_{\text{UV-fix IR}}$ between UV_{pump} and fixed IR_{pump} pulse. Left side, the pulse order is still correct (the gray pulse illustrates a possible position of the moving IR_{pump} pulse). Right side, the pulse order has changed since the IR_{pump} pulse moved within the defined coherence time delay.

The effect of this pulse order change within a measurement on the resulting T2D IR spectrum is not clarified yet. In Section 8.5, a close look at the measured data did not show a significant effect at that instant of time, where the UV_{pump} pulse interacts with the sample between the two IR_{pump} pulses. To circumvent the problem of changing pulse order within a measurement one could direct the UV_{pump} in the same way over the moving arm of the interferometer as the moving IR_{pump} pulse, such that the time delay $t_{\text{UV-mov. IR}}$ between these two pulses stays constant while changing the coherence time delay t_1, Fig. 48. In return, the time delay $t_{\text{UV-fix IR}}$ between the fix IR_{pump} and UV_{pump} pulse will change as well as the time delay between the UV_{pump} and IR_{probe} pulse. Therefore the so far, well-defined time delay between the UV excitation of the sample and IR probing will no longer be constant during a measurement.

The measurements presented in Section 8.4 outline the influence of different polarization between the IR_{pump} and IR_{probe} pulses. The polarization of the UV beam can additionally be changed by inserting a λ-half wave plate into the UV beam. The additional parameter concerning the polarization of the UV beam will give rise to other effects due to different polarizations settings of the beams. [23, 45]

A future task concerns the improvement of the sensitivity which is limited by the pump-probe geometry (Section 5). The probe beam is identical with the local oscillator such that the saturation of the detector limiting the intensity of the local oscillator also limits the probe beam intensity. W. Xiong and M. T. Zanni pointed out that polarization can be used to independently control the strength of all four fields even in the pump-probe geometry. [51] Orthogonal polarization of the two IR_{pump} pulses can be achieved by replacing the beam splitters by polarizing beam splitters (grid polarizer). A third polarizer is then placed behind the sample to block most of the probe beam but fully transmits the 3^{rd}-order polarization that is orthogonal to it. [34] For this purpose, already two optic mounts have been designed for grid polarizer's instead of the so far used beam splitters (Appendix A.2). The exchange of the beam splitters by grid polarizer's does not require significant realignment since only the mounts have to be replaced. In principle, the use of these grid polarizer's should enable the same sensitivity as the Photon-Echo method. [34]

To conclude, the T2D IR spectroscopy method based on a modified Mach-Zehnder interferometer build as part of this master thesis provides reliable T2D and 2D spectra with a maximal spectral resolution. It has been particularly taken care of that the experimental handling of the setup remains simple. Therefore, the Interferometer method describes a promising alternative to the established Fabry-Perot and Photon-Echo methods for 2D and T2D experiments.

A Technical Appendix

A.1 Frequency divider device

A light chopper within the UV beam is used to block the UV pump beam periodically to determine the T2D IR spectrum as described in Section 6 and 7. The T2D IR Interferometer method alternatively blocks three UV_{pump} pulses as discussed in Section 7.1.1 such that the light chopper has to run at a frequency equal to 1/6 of the repetition rate of the laser. A frequency divider was designed to obtain the desired frequency with respect to the laser repetition rate.
The designed frequency divider allows not only to divide the incoming frequency by six but uses a switch which allows the division of incoming frequency by 1, 2, up to 10. This feature is very convenient as the frequency divider device allows a easy switch between different UV_{pump} pulse blocking schemes (Section 7.1.1). Furthermore, the device can be used for other applications. Fig. 49(a) shows the circuit diagram using a "Johnson decade counter with 10 decoded outputs" and Fig. 49(b) shows a picture of the frequency divider device.

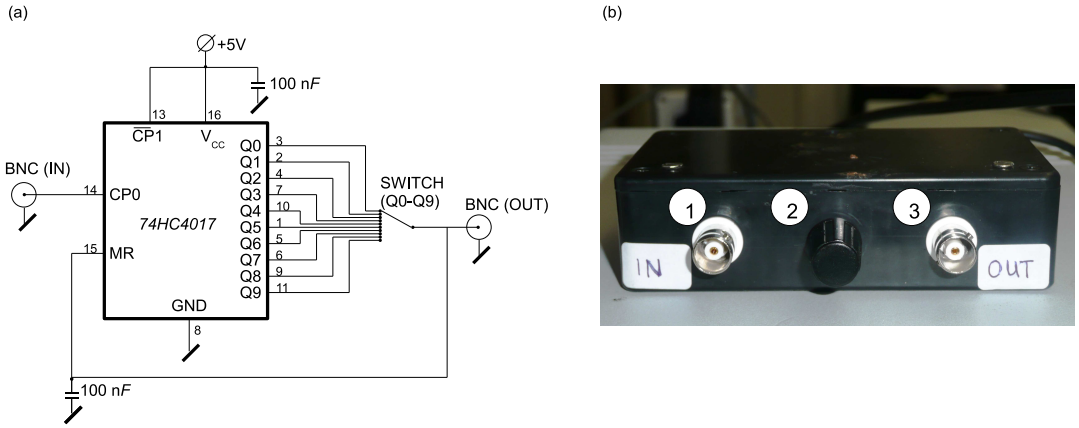

Figure 49: (a) Circuit diagram of the frequency divider. The main part of this design is the *"Johnson decade counter with 10 decoded outputs"* (74HC4017) which divides the incoming signal. (b) Picture of the frequency divider device: (1) frequency input BNC, (2) switch, (3) frequency output BNC.

A.2 Mounts for optics in the interferometer

The modified Mach-Zehnder interferometer in the T2D/2D setup is designed such that it can be used for a variety of experiments with a minimum of alignment. Therefore the interferometer can be modified easily. The mounts for the optics can be easily removed and exchanged such that for different optics only new mounts have to be designed and then replaced.

The experiments performed and presented use CaF_2 50:50 beam splitter within the IR beam. The designed mounts for these optics are shown in Fig. 51.
As mentioned in Section 9, in a future project the mid-IR beams splitters might be exchanged by grid polarizer's. Therefore, new mounts have been designed for the differently shaped grid polarizer's, Fig. 52, such that the new experiments can be performed with a minimum of realignment as only the new optics have to be inserted.

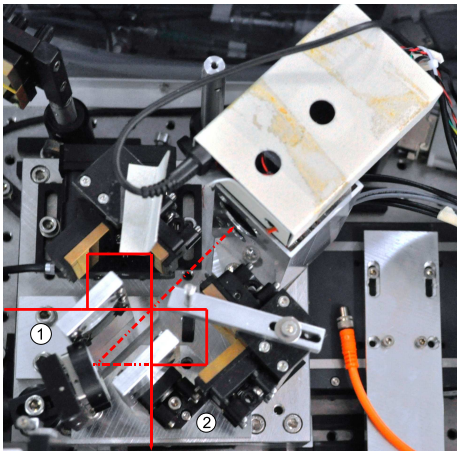

Figure 50: Picture of the interferometer with the mounts holding the optics (1,2). The mounts allow an easy exchange of optics for different experiments with a minimum of realignment.

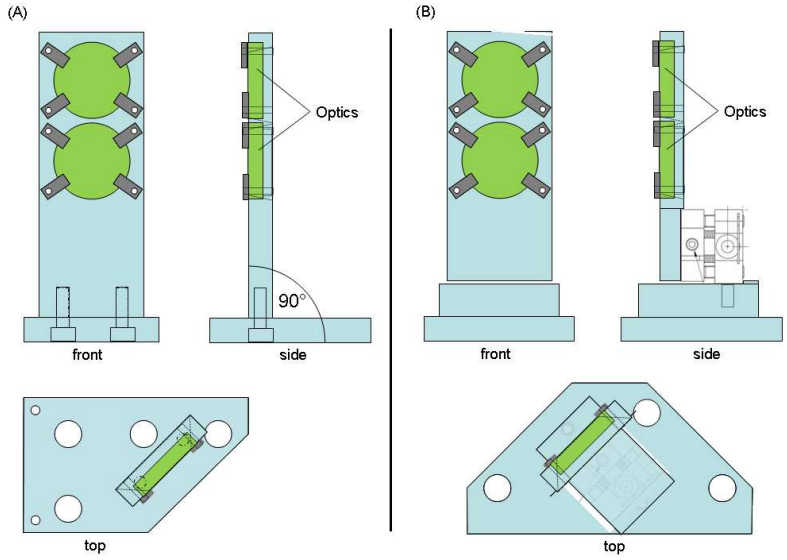

Figure 51: Illustration of the beam splitter mounts for the CaF_2 beam splitters (Thorlabs: CaF_2 Broadband Plate Beamsplitters (2-8 μm)) in the mid-IR beam and the broad band UV beam splitters (Thorlabs: UV Fused Silica Broadband Plate Beamsplitters (Coating: 400 - 700 nm)) in the HeNe beam.

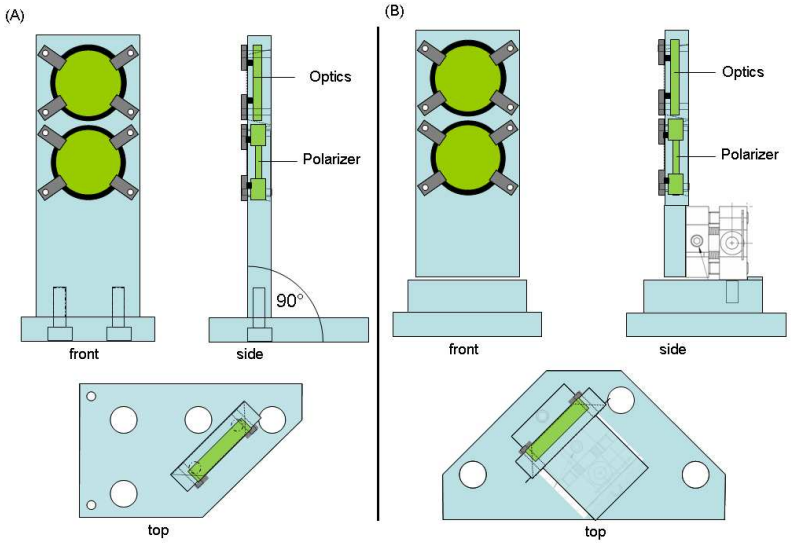

Figure 52: The grid polarizer mounts are designed for the same beam splitters in the HeNe beam and the wire-grid polarizer's (Thorlabs: BaF_2 Holographic Wire Grid Polarizer (WP25H-B)) in the mid-IR beam.

References

[1] P. Hamm, M. Lim, and R. M. Hochstrasser. Structure of the Amide I Band of Peptides Measured by Femtosecond Nonlinear-Infrared Spectroscopy. *J. Phys. Chem. B*, 102:6123–6138, 1998.

[2] W. P. Aue, E. Bartholdi, and R. R. Ernst. Two-dimensional spectroscopy. Application to nuclear magnetic resonance. *J. Phys. Chem. B*, 64(5):2229–2246, 1976.

[3] O. Golonzka, M. Khalil, N. Demirdöven, and A. Tokmakoff. Vibrational Anharmonicities Revealed by Coherent Two-Dimensional Infrared Spectroscopy. *Phys. Rev. Lett.*, 86(10):2154–2157, 2001.

[4] J. Bredenbeck, J. Helbing, and P. Hamm. Labeling Vibrations by Light: Ultrafast Transient 2D-IR Spectroscopy Tracks Vibrational Modes during Photoinduced Charge Transfer. *J. Am. Chem. Soc.*, 126:990–991, 2004.

[5] V. Cervetto, J. Helbing, J. Bredenbeck, and P. Hamm. Double-resonance versus pulsed Fourier transform two-dimensional infrared spectroscopy: An experimental and theoretical comparison. *J. Chem. Phys.*, 121(12):5935–5942, 2004.

[6] J. Zheng, K. Kwak, and M. D. Fayer. Ultrafast 2D IR Vibrational Echo Spectroscopy. *Acc. Chem. Res.*, 40:75–83, 2007.

[7] L. P. DeFlores, R. A. Nicodemus, and A. Tokmakoff. Two-dimensional Fourier transform spectroscopy in the pump-probe geometry. *Opt. Lett.*, 32(20):2966–2968, 2007.

[8] S.-H. Shim, D. B. Strasfeld, Y. L. Ling, and M. T. Zanni. Multidimensional Ultrafast Spectroscopy Special Feature: Automated 2D IR spectroscopy using a mid-IR pulse shaper and application of this technology to the human islet amyloid polypeptide. *Proc. Natl. Acad. Sci. U.S.A.*, 104(36):14197–14202, 2007.

[9] P. Hamm, M. Lim, W. F. DeGrado, and R. M. Hochstrasser. The two-dimensional IR nonlinear spectrsocopy of a cyclic penta-peptide in relation to its three-dimensional structure. *Proc. Natl. Acad. Sci. U.S.A.*, 96:2036–2041, 1999.

[10] S. Woutersen and P. Hamm. Nonlinear two-dimensional vibrational spectroscopy of peptides. *J. Phys.: Condens. Matter*, 14(39):R1035–R1062, 2002.

[11] O. Golonzka, M. Khalil, N. Demirdöven, and A. Tokmakoff. Coupling and orientation between anharmonic vibrations characterized with two-dimensional infrared vibrational echo spectroscopy. *J. Chem. Phys.*, 115, 2001.

[12] J. Bredenbeck and P. Hamm. Peptide structure determination by two-dimensional infrared spectroscopy in the presence of homogeneous and inhomogeneous broadening. *J. Chem. Phys.*, 119(3):1569–1578, 2003.

[13] S. Woutersen, Y. Mu, G. Stock, and P. Hamm. Subpicosecond conformational dynamics of small peptides probed by two-dimensional vibrational spectroscopy. *Proc. Natl. Acad. Sci. U.S.A.*, 98(20):11254–11258, 2001.

[14] S. Woutersen, Y. Mu, G. Stock, and P. Hamm. Hydrogon-bond lifetime measured by time-resolved 2D-IR spectroscopy: *N*-methylacetamide in methanol. *Chem. Phys.*, 266:137–147, 2001.

[15] N. Demirdöven, M. Khalil, and A. Tokmakoff. Correlated Vibrational Dynamics Revealed by Two-Dimensional Infrared Spectroscopy. *Phys. Rev. Lett.*, 89(23):237401, 2002.

[16] J. B. Asbury, T. Steinel, C. Stromberg, K. J. Gaffney, I. R. Piletic, A. Goun, and M. D. Fayer.

[17] M. Khalil, N. Demirdöven, and A. Tokmakoff. Coherent 2D IR Spectroscopy: Molecular Structure and Dynamics in Solution. *J. Phys. Chem. A*, 107:5258–5279, 2003.

[18] J. Bredenbeck, J. Helbing, R. Behrendt, Ch. Renner, L. Moroder, J. Wachtveitl, and P. Hamm. Transient 2D-IR spectroscopy: Snapshots of the Nonequilibrium Ensemble during the Picosecond Conformational Transition of a Small Peptide. *J. Phys. Chem. B*, 107(33):8654–8660, 2003.

[19] S. Woutersen, R. Pfister, P. Hamm, Y. Mu, D.S. Kosov, and G. Stock. Peptide conformational heterogeneity revealed from nonlinear vibrational spectroscopy and molecular-dynamics simulations. *J. Chem. Phys.*, 117:6833–6840, 2002.

[20] P. Hamm, J. Helbing, and J. Bredenbeck. Two-Dimensional Infrared Spectroscopy of Photoswitchable Peptides. *Annu. Rev. Chem. Phys.*, 59:291–317, 2008.

[21] J. B. Asbury, Y. Wang, and T. Lian. Time-Dependent Vibration Stokes Shift during Solvation: Experiment and Theory. *Bull. Chem. Soc. Jpn.*, 75:973–983, 2002.

[22] Y. Wang, J. B. Asbury, and T. Lian. Ultrafast Excited-State Dynamics of $Re(CO)_3Cl(dcbpy)$ in Solution and on Nanocrystalline TiO_2 and ZrO_2 Thin Films. *J. Phys. Chem. A*, 104:4291–4299, 2000.

[23] J. Bredenbeck, J. Helbing, and P. Hamm. Transient two-dimensional infrared spectroscopy: Exploring the polarization dependence. *J. Chem. Phys.*, 121(12):5943–5957, 2004.

[24] C. Kolano, J. Helbing, M. Kozinski, W. Sander, and P. Hamm. Watching hydrogen-bond dynamics in a β-turn by transient two-dimensional infrared spectroscopy. *Nature*, 444(7118):469–472, 2006.

[25] P. Hamm, R. A. Kaindl, and J. Stenger. Noise suppression in femtosecond mid-infrared light sources. *Opt. Lett.*, 25(24), 2000.

[26] Shaul Mukamel, editor. *Priniciples of Nonlinear Optical Spectroscopy.* Oxford University Press, Inc., 1. edition, 1995.

[27] Peter Hamm and Martin Zanni, editors. *Concepts and Methods of 2D Infrared Spectroscopy.* Cambridge University Press, 1. edition, 2011.

[28] M. C. Asplund, M. T. Zanni, and R. M. Hochstrasser. Two-dimensional infrared spectroscopy of peptides by phase-controlled femtosecond vibrational photon echoes. *Proc. Natl. Acad. Sci. U.S.A.*, 97(15):8219–8224, 2000.

[29] P. Hamm, M. Lim, and R. Hochstrasser. Non-Markovian Dynamics of the Vibration of Ions in Water from Femtosecond Infrared Three-Pulse Photon Echoes. *Phys. Rev. Lett.*, 81:5326–5329, 1998.

[30] M. Khalil, N. Demirdöven, and A. Tokmakoff. Obtaining Absorptive Line Shapes in Two-Dimensional Infrared Vibrational Correlation Spectra. *Phys. Rev. Lett.*, 90(4):047401, 2003.

[31] G. D. Goodno and G. Dadusc. Ultrafast heterodyned-detected transient-grating spectroscopy using diffractive optics. *J. Opt. Soc. Am. B*, 15(6):1791–1794, 1998.

[32] U. Selig, F. Langhojer, F. Dimler, T. Löhrig, C. Schwarz, B. Gieseking, and T. Brixner. Inherently phase-stable coherent two-dimensional spectroscopy using only conventional optics. *Opt. Lett.*, 33(23):2851–2853, 2008.

[33] E. H. G. Backus, S. Garrett-Roe, and P. Hamm. Phasing problem of heterodyne-detected two-dimensional infrared spectroscopy. *Opt. Lett.*, 33(22):2665–2667, 2008.

[34] J. Helbing and P. Hamm. Compact implementation of Fourier transform two-dimensional IR spectroscopy without phase ambiguity. *J. Opt. Soc. Am. B*, 28(1):171–178, 2011.

[35] J. Bredenbeck, J. Helbing, and P. Hamm. Two-dimensional IR spectroscopy of transient species. *Opt. Soc. of Am.*, 2004.

[36] F. Perakis and P. Hamm. Two-Dimiensional Infrared Spectroscopy of Supercooled Water. *J. Phys. Chem. B*, 115:5289–5293, 2011.

[37] F. Perakis, S. Widmer, and P. Hamm. Two-dimensional infrared spectroscopy of isotope-diluted ice lh. *J. Chem. Phys.*, 134:204505, 2011.

[38] J. Bredenbeck, J. Helbing, and P. Hamm. Continuous scanning from picoseconds to microseconds in time resolved linear and nonlinear spectroscopy. *Rev. Sci. Inst.*, 75(11):4462–4466, 2004.

[39] A. W. Albrecht, J. D. Hybl, S. M. G. Faeder, and D. M. Jonas. Experimental distinction between phase shifts and time delays: implications for femtosecond spectroscopy and coherent control of chemical reactions. *J. Chem. Phys.*, 111:10934–10956, 1999.

[40] R. Bloem, S. Garret-Roe, H. Strzalka, P. Hamm, and P. Donaldson. Enhancing signal detection and completely eliminating scattering using quasi-phase-cycling in 2D IR experiments. *Opt. Express*, 18(26):27067–27078, 2010.

[41] M. J. Downs and K. W. Raine. An unmodulated bi-directional fringe-counting interferometer system for measureing displacement. *Precis. Eng.*, 1:85–88, 1979.

[42] L. Lepetit, G. Chériaux, and M. Joffre. Linear techniques of phase measurement by femtosecond spectral interferometry for applications in spectroscopy. *J. Opt. Soc. Am. B*, 12:2467, 1995.

[43] J. Bredenbeck. *Transient 2D-IR Spectroscopy - Towards Ultrafast Structural Dynamics of Peptides and Proteins.* PhD thesis, University of Zurich, 2005.

[44] J. Bredenbeck and P. Hamm. Versatile small volume closed-cycle flow cell system for transient spectroscopy at high repetition rates. *Rev. Sci. Instrum.*, 74(6):3188–3189, 2003.

[45] M. T. Zanni, N.-H. Ge, Y. S. Kim, and R. M. Hochstrasser. Two-dimensional IR spectroscopy can be designed to eliminate the diagonal peaks and expose only the crosspeaks needed for structure determination. *Proc. Natl. Acad. Sci. U.S.A.*, 98(20):11265–11270, 2001.

[46] L. A. Worl, R. Duesing, P. Chen, L. D. Ciana, and T. J. Meyer. Photophysical Properties of Polypyridyl Carbonyl Complexes of Rhenium(I). *J. Chem. Soc., Dalton Trans.*, pages 849–858, 1991.

[47] J. Bredenbeck, J. Helbing, and P. Hamm. Solvation beyond the Linear Response Regime. *Phys. Rev. Lett.*, 95(8):083201, 2005.

[48] R. M. Hochstrasser. Two-dimensional IR-spectroscopy: polarization anisotropy effects. *Chem. Phys.*, 266:273–284, 2001.

[49] H. S. Chung, Z. Ganim, K. C. Jones, and A. Tokmakoff. Multidimensional Ultrafast Spectroscopy Special Feature: Transient 2D IR spectroscopy of ubiquitin unfolding dynamics. *Proc. Natl. Acad. Sci. U.S.A.*, 104(36):14237–14242, 2007.

[50] H. S. Chung, M. Khalil, A. W. Smith, and A. Tokmakoff. Transient two-dimensional IR spectrometer for probing nanosecond temperature-jump kinetics. *Rev. Sci. Inst.*, 78(6):063101, 2007.

[51] W. Xiong and M. T. Zanni. Signal enhancement and background cancellation in collinear two-dimensional spectroscopies. *Opt. Lett.*, 33(12):1371–1373, 2008.

Acknowledgements

Many individuals supported me during the completion of this master thesis and I would like to take this opportunity to express my gratitude to all of them.
I would like to thank Prof. Dr. Peter Hamm for giving me the chance to carry out my master thesis in his research group at the Institute of Physical Chemistry (PCI) at the University of Zürich and the coordinator from the Physics Institute, Prof. Dr. Andreas Schilling for making it possible.
First and foremost I offer my sincerest gratitude to my supervisor, Dr. Jan Helbing who has supported me throughout my thesis with his patience and endurance to explain all aspects of spectroscopy and physics and for contributing with his talent and skills.
I would like to thank every member of this research group for their assistance, constructive criticisms and useful insights. I felt very well supported from the first day. I had always the possibility to go and ask everyone for advice or help.
A special mention goes to my colleagues Julien Réhault, Fivos Perakis, Marco Schade, and Biplab Dutta who worked with me in the same laboratory and were on hand with help and advice. I would also particularly like to thank my office mates Dr. Janne Savolainen and Joanna Borek for all the discussion (serious and less serious) which provided a great atmosphere. I especially thank Joanna for all the great deserts she made.
Many thanks go to the staff of the PCI Institute for providing an excellent infrastructure and especially to our technicians, Armin Kühne, Roland Zehnder and Martin Haller. I was often surprised how quickly and efficiently all types of technical problems were solved.
I thank Sascha Giger for all the IT support and Maja Grossweiler who manages all the administrative jobs.
A special mention goes to Michael Schindlberger who became a very good friend on our venture towards my master degree.
Finally, this thesis would not have been possible without the confidence, patience and support of my family. They have always encouraged me throughout my entire studies. I wish to thank my parents, Uschi and Felix, whose love, teachings and support have brought me this far. I thank my brother Benny for all his support, encouragement and advices. I especially wish to thank my girlfriend Ivana for her affection, understanding and patience.